

Peaks and cusps: anomalous thresholds and LHC physics

Giampiero Passarino^a

^a*Dipartimento di Fisica Teorica, Università di Torino, Italy
INFN, Sezione di Torino, Italy*

Abstract

The behavior of scattering amplitudes in the vicinity of a physical-region Landau singularity is considered. The impact on LHC processes is discussed.

Keywords: LHC physics; Feynman diagrams; Landau singularities

PACS: 11.55.Bq, 12.15.Lk, 11.15.Bt

1. Introduction

Resonances are normally observed as peaks in certain invariant mass distributions; however, a question arises: is a peak necessarily due to the presence of a resonance? Are there peaks produced by kinematic singularities?

Landau equations for a given Feynman integral are a set of kinematic constraints that are necessary for the appearance of a pole or branch point in the integrated function (as a function of external kinematics and masses). Landau equations admit many families of solutions which are naturally classified as leading Landau singularities (LLS), sub-leading Landau singularities (SLLS), sub-sub-leading (S²LLS) etc.

Leading Landau singularities have been studied mostly in the context of hadron spectroscopy [1] where, in order to establish an unambiguous strategy it is important to distinguish kinematic singularities from genuine resonances, i.e. poles of the S-matrix. An example is $B^+ \rightarrow B_s^0 \pi^+ \pi^0$ via $B\bar{K}^*$ rescattering [2, 3].

As an example, a triangle singularity is a logarithmic branch point, which would produce an infinite reaction rate if it appears in the physical region. This never happens because at least one of the three particles must be unstable. The finite width, introduced by the complex-mass scheme [4–6], moves the singularity into the complex plane, and the differential reaction rate can have a finite peak due to the proximity of the singularity. Here, by complex plane we mean complex plane for Mandelstam invariants or complex hypersurface in the parametric representation of the corresponding diagram, i.e. no pinch singularity in Feynman parameter space.

The subject of Feynman amplitudes with variable momenta and non-zero masses has been studied by physicists since the 1950's, e.g. the inelastic scattering $K^+ + p \rightarrow \pi^+ + \pi^0 + p$ (see Figs.[1,2] of Ref. [7]). Meanwhile new mathematical methods involving Hodge structures and variations of Hodge structures have been developed. The use of these techniques to the study of amplitudes and Landau singularities in momentum space has been described in Refs. [8, 9]. A determination of the complete set of branch points of amplitudes in planar $N = 4$ super-Yang-Mills theory directly from the amplituhedron, without resorting to any particular representation in terms of local Feynman integrals has been presented in Ref. [10].

Email address: giampiero@to.infn.it (Giampiero Passarino)

However, in recent years, not much attention has been paid to the problem in the context of high energy physics, with the noticeable exception of the work by Boudjema and collaborators [11–13] (see also section 4.4 of Ref. [14], Ref. [15] and developments in the Golem95 project, e.g. Ref. [16]).

In this paper we analyze typical LHC processes looking for possible effects due to the presence of a leading Landau singularity, or anomalous threshold (hereafter AT). It should be stressed that by “cusp” we mean a cusp in some differential distribution (e.g. invariant mass or p_T) and not cusp of a Landau variety ¹.

In the rest of this paper we discuss the complications that arise in dealing with the singular part of a scattering amplitudes and the impact of anomalous thresholds on LHC physics. We begin in section 2 by reviewing briefly the definition of leading Landau singularities, illustrating the introduction of complex masses.

In section 3 – section 7 we describe LLS for two-, three-, ... six-point functions using the complex mass scheme discussed in subsection 2.1. In section 8 we include two-loop diagrams into our analysis. In section 9 we discuss special configurations leading to non-integrable LLS, even within the regularization introduced by complex masses. QED/QCD induced LLS, not to be mistaken for the infrared ones, are presented in subsection 4.1. In section 10 we discuss relatively simple examples of beyond-standard-model (BSM) LLS. In Appendix A – Appendix B technical details are presented.

2. Leading Landau singularities

Learning from the study of singularities of scattering amplitudes:

- ① For a given Feynman diagram there exists a discriminant

$$D(p_i \cdot p_j, m_i^2, \alpha_i), \quad (1)$$

which is an homogeneous polynomial in the α_i and whose coefficients are linear in the $p_i \cdot p_j$ ² and m_i^2 , such that the equations $\partial D / \partial \alpha_i = 0$ are equivalent to the usual Landau conditions for the existence of the singularity, as described in Ref. [18]. As it is well known, given any m homogeneous polynomials in m unknowns there exists a unique minimal homogeneous polynomial in the coefficients (R the resultant) such that $R = 0$ is a necessary and sufficient condition for the existence of a solution to the system of equations (Landau-Nakanishi equations), distinct from the trivial solution $\alpha_1 = \dots \alpha_m = 0$ ³. Note that $\alpha_i \geq 0$ is required for the scattering to be physical (the so-called $+\alpha$ Landau surfaces, as opposite to “mixed- α ” solutions).

- ② The leading Landau singularity requires all of the α_i 's to be non zero; the case where some of the parameters vanish can be interpreted as the leading singularity of a diagram obtained from the original one contracting the lines associated to the vanishing α 's. Note that the definition used in Ref. [27] differs slightly from our conventional usage. Furthermore, for a given set of values (p_1, \dots, p_N) which lie on the given physical-region Landau singularity there exists only one unique set of values for the internal momenta which satisfy the Landau equations.

For the discussion of LL singularities there are three important theorems.

Theorem 2.1 (Coleman and Norton [28]). *A Feynman amplitude has singularities on the physical boundary if and only if the relevant Feynman diagram can be interpreted as a picture of an energy- and momentum-conserving process occurring in space-time, with all internal particles real, on the mass shell, and moving forward in time. As a by-product, the Feynman parameter associated with an internal line is identified (within a proportionality factor) with the time the particle exists between collisions, divided by its mass.*

¹A Landau variety L is a reducible algebraic variety; the singular points of a generic plane section of L are expected to be transverse intersections, tacnodes or cusps [17].

²In our metric, space-like p corresponds to positive p^2 . Further $p_4 = i p_0$ with p_0 real for a physical four-momentum.

³Usually Landau-Nakanishi [19, 20] equations are called Landau equations for short, see also Bjorken (thesis, Stanford Univ. 1959) and Refs. [21–26]

Additional results can be found in Refs. [29–34]. Other results can be found in Ref. [35], where it is stressed that the meaning of “physical boundary” in the Coleman-Norton theorem is as follows: consider the triangle of Figure 3, the unitary cut starts at $(m_1 + m_3)^2$ (right-hand branch cut); the physical boundary is just above the cut. To give an example, the original Peierls mechanism [36] gives singularities on the wrong sheet; the modified Peierls mechanism [37] gives the (triangular) singularity on the correct sheet but it has been shown that does not produce peaks in invariant-mass plots, the so-called Schmid theorem [35]. Nevertheless, in Ref. [38] it was argued that terms involving the singularity of a triangle diagram can in principle at least lead to observable effects in the differential cross section. Other counterexamples can be found in Ref. [39] and in Refs. [40, 41]. However, one should be aware that most of these papers limit their analysis to triangular singularities.

Theorem 2.2 (Kershaw [42]). *The singular part of a scattering amplitude around its leading Landau singularity may be written as an algebraic product of the scattering amplitudes for each vertex of the corresponding Landau graph times a certain explicitly determined singularity factor which depends only on the type of singularity (triangle graph, box graph, etc.) and on the masses and spins of the internal particles.*

It is worth noting that the consequences of the theorem have been reinterpreted by various authors in terms of multiple cuts on Feynman diagrams [43–50].

Kershaw theorem is based on the fact that there always exists a finite polynomial in the scalar product of the external momenta such that $P(p_i \cdot p_j) = 0$ gives the location of the leading Landau singularity. The proof of this property is particularly simple for one-loop diagrams. Consider a scalar, one-loop, N-point functions in d dimensions ($d = 4 - \varepsilon$): external momenta will be labelled as p_1, \dots, p_N and let us consider \mathcal{P}_N the set of the non-cyclic permutation of $(1, \dots, N)$ with the first entry fixed. Vectors k_i are introduced according to the following convention:

N = 3 there are two elements, i.e. $(1, 2, 3)$ and $(1, 3, 2)$. We define

$$\begin{aligned} (1, 2, 3) &\rightarrow k_1 = p_1, k_2 = p_2, \\ (1, 3, 2) &\rightarrow k_1 = p_1, k_2 = p_3. \end{aligned} \quad (2)$$

N = 4 There are three elements and we define

$$\begin{aligned} (1, 2, 3, 4) &\rightarrow k_1 = p_1, k_2 = p_2, k_3 = p_3, \\ (1, 2, 4, 3) &\rightarrow k_1 = p_1, k_2 = p_2, k_3 = p_4, \\ (1, 3, 2, 4) &\rightarrow k_1 = p_1, k_2 = p_3, k_3 = p_2. \end{aligned} \quad (3)$$

N = 5 There are twelve elements, etc.

With the notations of Ref. [51] we define a scalar integral as

$$S_{d;N}(w) = \frac{\mu^\varepsilon}{i\pi^2} \int d^d q \frac{1}{\prod_{i=0, N-1} [i]}, \quad [i] = (q + k_0 + \dots + k_i)^2 + m_i^2, \quad (4)$$

where $k_0 = 0$ and where w is an element of \mathcal{P}_N . Furthermore μ is the 't Hooft scale and $\varepsilon = d - 4$. In this way we can characterize the whole set of N-point functions contributing to a given amplitude and not just one specific diagram.

In parametric space we obtain

$$S_{dN}(w) = \left(\frac{\mu^2}{\pi}\right)^{2-d/2} \Gamma(N - \frac{d}{2}) [N]_d(w), \quad (5)$$

where from the triangle to the hexagon we will use the following notations: $[3] \equiv C, \dots, [7] \equiv G$. We have

$$[N]_d(w) = \int dS_{N-1} V_N^{d/2-N}(w), \quad (6)$$

$$V_N(w) = x^t H_N(w) x + 2 K_N^t(w) x + L_N(w), \quad X_N(w) = -K_N^t(w) H_N^{-1}(w), \quad (7)$$

$$\Delta_N(w) = L_N(w) - K'_N(w) H_N^{-1}(w) K_N(w), \quad (8)$$

where $H_{ij} = -k_i \cdot k_j$; $G_N = \det H_N$ is the Gram determinant associated with the N-point function of argument $w \in \mathcal{P}_N$. Furthermore, $K_i = -1/2(m_i^2 - m_{i+1}^2 - k_i^2 - 2 \sum_{j=1, i-1} k_j \cdot k_i)$, $L = m_1^2$ and

$$\int dS_{N-1} = \int_0^1 dx_1 \int_0^{x_1} dx_2 \dots \int_0^{x_{N-2}} dx_{N-1}. \quad (9)$$

Let M_N be the $N \times N$ matrix

$$M_N = \begin{pmatrix} H_N & K_N \\ K'_N & L_N \end{pmatrix}$$

Then one can easily prove that

$$\Delta_N(w) = \frac{C_N(w)}{G_N(w)}, \quad X_N^i = \frac{\det M_{(i, N)}}{G_N}, \quad (10)$$

where $C_N = \det M_N$ is the so-called modified Cayley determinant [52, 53] of the diagram ⁴ and we can write

$$V_N = (x - X_N)^t H_N (x - X_N) + \Delta_N = y^t M_N y, \quad (11)$$

where $y^t = (x^t, 1)$.

Theorem 2.3 (Ferrogia et al. [51]; Gorla and Passarino [55]). *It is easily seen ⁵ that $\Delta_N = 0$ induces a pinch [57–59] on the integration contour at the point $x = X_N$; therefore, if*

$$\Delta_N = 0, \quad 0 < X_{N, N-1} < \dots < X_{N, 1} < 1, \quad (12)$$

we have the leading singularity (from Eq.(11) we derive that it represents a singular point of multiplicity two). Leading singularities of diagrams obtained by shrinking one (or more) line of the original diagram to a point give the sub-leading singularities.

In the Cayley language the Landau equations for a general case can be written as follows. Consider the integral

$$I = \int_D \prod_{i=1}^n dx_i V_{N, n}^{-\mu}(x_1 \dots x_n; w_1 \dots w_k), \quad (13)$$

where V is a multivariate polynomial of degree N and an algebraic function of k -parameters $w_1 \dots w_k$. Therefore $V \in \mathbb{C}[x, w]$. D is the domain of integration. $V_{N, n} = 0$ is the locus of the singularities of the integrand; let $\mathcal{B}_j(x, w)$, $j = 1, \dots, d$ be the set representing the boundary of D .

Proposition 2.4. *The necessary conditions for the leading singularities to occur when the hypercontour is pinched between the surfaces of singularity or meets a boundary variety are*

○ $\exists \alpha_i, \beta$, not all equal to zero and such that at the point $w_k = w_k^0$ and $x_k = x_k^0$ we have $\beta V_{N, n} = 0$ and

$$\begin{aligned} \alpha_i \mathcal{B}_i(x_i, w_i) &= 0, \quad i = 1, \dots, d, \\ \frac{\partial}{\partial x_i} \left[\sum_i \alpha_i \mathcal{B}_i(x, w) + \beta V_{N, n}(x, w) \right] &= 0, \quad i = 1, \dots, n. \end{aligned} \quad (14)$$

⁴The more familiar definition is as follows: define propagators $[i] = (q + q_i)^2 + m_i^2$, with $q_0 = 0$; introduce the matrix $Y_{ij} = 1/2((q_i - q_j)^2 + m_i^2 + m_j^2)$ and define the modified Cayley determinant as $C = \det Y$. To be more precise C is proportional to a signed minor [54] of the modified Cayley determinant defined in Ref. [52, 53].

⁵In general for a hypersurface $V(x_1 \dots, x_n) = 0$ the singular points are those at which all the partial derivatives simultaneously vanish. The notion of singular points is a purely local property. The determination of the multiplicity of a singular point, is based on ascertaining which of the higher-order derivatives vanish at that point [56].

If D is a n -dimensional hypercube and

$$V_{N,n} = \sum_{i=0}^N V_n^i, \quad V_n^i = \sum_{0 \leq i_1 = \dots = i_n \leq i} a_{i_1 \dots i_n}^i x_1^{i_1} \dots x_n^{i_n}, \quad (15)$$

where the V_n^i are homogeneous polynomials and $V_{N,n}$ is a generic polynomial in the ring of polynomials of degree N , it is convenient to determine the $(N-1)^n$ n -tuples $X_1^i \dots X_n^i$ such that

$$V_{N,n}(x_1 - X_1^i \dots x_n - X_n^i) = \Delta + \sum_{i=2}^N V_n^i(x_1 - X_1^i \dots x_n - X_n^i), \quad i = 1 \dots (N-1)^n, \quad (16)$$

so that the solutions of $\Delta(w_1 \dots w_k) = 0$, are the potential (leading) pinch singularities if $X_j^i \in \mathbb{R}$, $0 < X_j^i < 1 \forall j$. For $V_n^2 = \dots = V_n^k = 0$ the singular point will have multiplicity $k+1$.

To summarize: a general understanding of the behavior of Feynman amplitudes may be obtained by analogy with the behavior of a function f of a single complex variable z , defined as a contour integral with respect to a second variable s of a function g analytic in z and s . The singularities of $f(z)$ arise for values of z for which two singularities of $g(z, s)$ coincide in the s plane, trapping the contour of integration. A general point on a Landau singularity corresponds to the occurrence in the integration space of the analog of this mechanism for functions of several complex variables. The extension to more than one external variables and the situations where a pinch may become harmless (e.g. falling off the end of the contour) are discussed in chapter 2.1 of Ref. [57]; the extension to multiple integrals can also be found there and in Eq.(14).

There also exist ‘‘second-type’’ (so-called non-Landau) singularities (see for example Ref. [57]). These arise in Feynman loop integrals as pinch singularities at infinite loop momentum and will not be analyzed in this work.

More details on Landau singularities.

For more details from the point of view of algebraic geometry see Refs. [17, 53]. Landau equations in the context of the theory of asymptotic operation have been discussed in Ref. [60]. Finally, solutions to the Landau conditions, corresponding to kinematic configurations where the modified Cayley determinant vanishes, are called singularities of the first type (singularities of the first type comprise all solutions to the Landau conditions for finite values of loop momentum); for a geometric interpretation in terms of volumes of polytopes see Ref. [61]. For an interpretation in terms of projective geometry and momentum twistors see Ref. [62]. For the analyticity properties of amplitudes in theories with nonlocal vertices of the type occurring in string field theory see Ref. [63]. For Landau diagrams in theories with gravity duals see Ref. [64]. Furthermore, for amplitudes of generalized polylogarithm type there should be a close connection between symbol entries and solutions of the Landau equations [64]. The most recent developments deal with massless theories which is of no help here since, in our case, at least one internal line must have nonzero mass.

Another description of the AT is as follows: 3 and higher point functions can be cut in more than two pieces; putting all propagators on-shell corresponds to $\alpha_i \neq 0$ at the level of the Landau equations, i.e. ATs go beyond the concept of unitarity cuts [7, 65, 66]. For an alternative proof of cutting rules in quantum field theories see Ref. [67].

Vanishing Cayley determinants have been mentioned in the literature but, usually, this case has not been considered in detail since ‘‘the exceptional case with a vanishing modified Cayley determinant hardly appears in applications’’, see Refs. [54, 68]; however, reduction of tensor integrals for small Gram determinant and/or small modified Cayley determinant have been discussed in Ref. [69].

The expansion of Feynman integrals around their AT is easy to derive analytically and only requires Mellin-Barnes and sector decomposition techniques as explained in Ref. [51]. Examples of leading behavior (details are given in Appendix B) are: for the vertex $C_0 \sim \ln \Delta_3$; for the box $D_0 \sim \Delta_4^{-1/2}$; for the pentagon $E_0 \sim \Delta_5^{-1}$ and no singularity for the hexagon F_0 in 4 dimensions [57]; e.g. $\text{Im } C_0$ has a logarithmic singularity, $\text{Re } C_0$ has a discontinuity. Δ_n is analytic in the immediate vicinity of the given singularity and singular on it. Of course, we can add any function, analytic in the neighborhood of the singularity. The general result can be summarized as follows: let L be the number

of internal lines in the Feynman diagram under consideration and v the number of loops; define $\rho = 2v - 1/2(L + 1)$, the leading behavior of the diagram is given by (special cases are discussed in Appendix B)

$$\Delta_L^\rho \text{ for } \rho < 0, \quad \Delta_L^{k+1/2} \text{ for } \rho = k + \frac{1}{2}, \quad \Delta_L^k \ln \Delta_L \text{ for } \rho = k, \quad k \in \mathbb{Z}^*. \quad (17)$$

Therefore for $L = 2(2v + n) - 1$ and $n \in \mathbb{Z}^+$ the AT is a pole of order n for the amplitude, e.g. a simple pole for the one-loop pentagon, for two-loop diagrams with 9 propagators etc. In all other cases it is a branch point.

One-loop diagrams: summary Any one-loop diagram is specified by

- ① H_N , a $(N - 1) \times (N - 1)$ matrix whose determinant is the Gram determinant.
- ② The set $\{X_1, \dots, X_{N-1}\} = X_N$; we will denote by X_N^{ord} the set $\{(X_1, \dots, X_{N-1}) \in \mathbb{R}^{N+1} \mid 0 < X_{N-1} < \dots < X_1 < 1\}$.
- ③ The Bernstein-Sato-Tkachov [70–72] factor Δ_N defined in Eqs.(8)–(10). The Bernstein theorem [70] states that for any polynomial in $\mathbb{C}[x]$ there exists a non-zero polynomial $b(s) \in \mathbb{C}[s]$ (Bernstein-Sato polynomial [70, 71]) and a differential operator $P(s) \in D_n(s)$ such that $P(s) \cdot f^{s+1} = b(s)f^s$. For one-loop diagrams Δ_N is the explicit form of b , as shown in Ref. [72].
- ④ The set of generalized Mandelstam invariants, \mathbf{I} ; we will denote by \mathbf{I}_{phys} a set of invariants internal to the physical region⁶.

Real (complex) masses: anomalous threshold Assume that all masses are real ($\{\Gamma\} = 0$), the physical-region LLS (or physical-region anomalous threshold) is given by

$$\Delta_N \Big|_{\{\Gamma\}=0} = 0, \quad X_N = X_N^{\text{ord}}, \quad \{\mathbf{I}\} = \{\mathbf{I}\}_{\text{phys}}. \quad (18)$$

There are cases where the first two conditions are satisfied but Mandelstam invariants are moved to their complex plane. Nevertheless, their real part can be inside the physical region with a tiny imaginary part; therefore they can be very close to the boundary. When internal masses are made complex, i.e. $m_i^2 \rightarrow m_i^2 - i\Gamma_i m_i$, singularities move into the complex x -space. We are nevertheless interested in the following configurations:

$$\begin{aligned} \text{Re } \Delta_N &\approx \Delta_N \Big|_{\{\Gamma\}=0} \approx 0, & \text{Im } \Delta_N &\ll 1, \\ \{\text{Re } X_i\} &= \{\text{Re } X_i\}^{\text{ord}}, & \text{Im } X_i &\ll 1, \end{aligned}$$

with $\{\mathbf{I}\} = \{\mathbf{I}\}_{\text{phys}}$. The introduction of complex masses regularizes the singularity since, in general, $\text{Im } \Delta_N \neq 0$; however another special configuration is possible:

Peierls zeros [36] They are defined by

$$\text{Re } \Delta_N = \text{Im } \Delta_N = 0, \quad (19)$$

and we look for a set of “real” invariants that satisfy Eq.(19), possibly within the physical region and with $\{\text{Re } X_i\} = \{\text{Re } X_i\}^{\text{ord}}$. The effect of these zeros can be seen by considering a simple example:

$$F(y, z) = \int_{-1}^{+1} dx \left[(x + iy)^2 - z^2 \right]^{-1}, \quad (20)$$

where $y \in \mathbb{R}$ and $z \in \mathbb{C}$. We derive

$$F(y, z) = \frac{1}{2z} \left\{ \ln \left[(z-1)^2 + y^2 \right] - \ln \left[(z+1)^2 + y^2 \right] + \eta(z-1, z-1) \right\}$$

⁶In this paper “physical region” is identified with the phase space for the corresponding process, i.e. the physical region of a given process is the set of all real initial and final energy-momenta variables subject to the mass-shell conditions and to energy-momentum conservation. Solutions that correspond to points outside the physical region are on the wrong sheet.

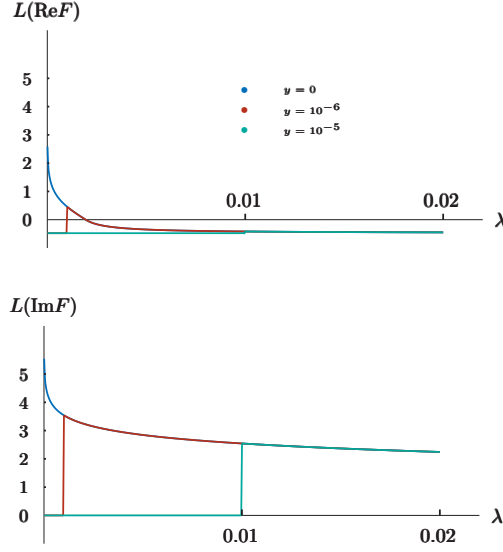


Figure 1: Real and imaginary part of $L(F)$ where F is given in Eq.(20) and L is the log-modulus function [74] defined in Eq.(40).

$$= \frac{1}{2z} \left[\ln \frac{z-1-iy}{z+1-iy} - \ln \frac{z+1+iy}{z-1+iy} \right], \quad (21)$$

where η is the 't Hooft-Veltman eta function [73] and the $\ln v$ denotes the principal branch, $-\pi < \arg(v) \leq +\pi$. If $z = \alpha + i\beta$ with $-1 \leq \alpha \leq +1$ and $\beta \geq 0$ we derive

$$F(0, z) \sim \frac{i\pi}{z}, \quad \text{for } z \rightarrow 0, \quad (22)$$

showing a pinch singularity for $z = 0$. When we set $z = 0$ with $y \neq 0$ we obtain

$$F(y, 0) = -\frac{2}{1+y^2}, \quad (23)$$

without a pinch, i.e. one double pole of the integrand at $x = -iy$ instead of two simple poles at $x = \pm z$. In general, let us consider

$$F(z_1, z_2) = \int_{-1}^{+1} dx \left[(x-z_1)^2 - z_2^2 \right]^{-1}, \quad (24)$$

where $z_{1,2}$ depend on real external parameters, s_1, \dots, s_n . Let Σ be the hypersurface in s -space where $z_2 = 0$; furthermore, let Π_+ be the hypersurface where $\text{Im} z_1 = 0$ and $-1 \leq \text{Re} z_1 \leq +1$. If we follow a path on Π_+ and approach Σ a pinch will appear; starting with a point in Σ and not in Π_+ and following any path on Σ will not give a pinch singularity.

To illustrate the behavior of $F(y, z)$ we fix $z = 0.9 + i10^{-3}$ and scale it with a factor λ , showing $F(y, \lambda z)$ as a function of λ for $y = 0, 10^{-6}, 10^{-5}$. The result is shown in Figure 1; for $y = 0$ the $1/z$ behavior in the imaginary part is evident. With small y there is no pole but a discontinuity (a large gap) is present, corresponding to a value of λ where the imaginary part of the first logarithm in Eq.(21) changes sign.

A more detailed discussion concerning boxes and pentagons will be given in section 9.

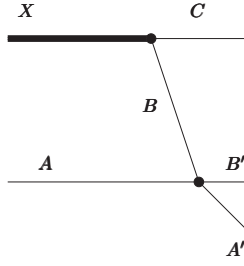


Figure 2: Diagram which generates the Brayshaw singularity [75, 76].

Analytic continuation As long as $\text{Im } X_i \neq 0$ there is no singularity, even if $\{\text{Re } X_i\} = \{\text{Re } X_i\}^{\text{ord}}$. In general the introduction of complex masses causes the singularity to be removed rather far from the real axis, i.e. the integral

$$\begin{aligned}
 [\text{N}]_n(w) &= \int dS_{\text{N}-1}^{\gamma} \mathbf{V}_{\text{N}}^{n/2-\text{N}}(w), \\
 \int dS_{\text{N}-1}^{\gamma} &= \int_0^1 dx_1 \int_0^{x_1} dx_2 \dots \int_0^{x_{\text{N}-2}} dx_{\text{N}-1},
 \end{aligned}
 \tag{25}$$

is regular if the paths γ_i , connecting 0 and x_{i-1} lie on the real axis. This indicates a branch point of the integral that is not present on the physical sheet but only becomes apparent after suitable analytic continuation away from the physical contour. However, there are circumstances where the singularity can be shifted very near (or even inside) the physical region defined by $\{\text{Re } X_i\} = \{\text{Re } X_i\}^{\text{ord}}$, with $\{\text{Im } X_i\} = 0$ and $\{\text{I}\} = \{\text{I}\}_{\text{phys}}$. In this case we will have the so-called Peierls or Brayshaw singularities [75, 76]. The scattering diagram generating the Brayshaw singularity is shown in Figure 2 where the blobs refer to off-shell scattering amplitudes and A', B' are at threshold while X is a resonance. Consider the s -plane for the X - A scattering, the Peierls singularity is a special case occurring at $s = 2(m_X^2 + m_A^2) - m_B^2$.

From Coleman-Norton theorem 2.1 and Kershaw theorem 2.2 we immediately realize that a physical-region singularity requires a theory with a hierarchy of heavy masses. Furthermore identical masses in a vertex must be avoided, e.g. X and C in Figure 2 cannot have the same mass; if we stay within the standard model this means that B cannot be neutral, a Z or a H boson. Therefore we are limited to consider only two heavy particles, the t -quark and the W -boson. Furthermore, anomalous thresholds in the standard model (SM) prefer the so-called “off-shell” region, e.g. gg producing an off-shell Higgs (with a virtuality greater than $2m_t$) subsequently “decaying” into four fermions, see Refs. [77, 78]. The situation changes when we consider BSM models as we will discuss later.

2.1. Complex masses

The so-called “complex-mass scheme” has been introduced and discussed (in modern times) in Refs. [4–6, 79] (for an introduction before the advent of gauge theories see Ref. [80]; analyticity in the complex mass shell has been discussed in Ref. [81]). An amplitude with unstable (internal) particles can be regarded as an analytic continuation of the amplitude defined by Feynman prescription.

One should remember that unstable states lie in a natural extension of the usual Hilbert space that corresponds to the second sheet of the S -matrix⁷; for instance we will have to take the logarithm of $z = z_R + iz_I$, where z is the polynomial occurring in the calculation of a given Feynman diagram and where, in the limit of zero widths, we have $z = z_0 - i0$. The analytic continuation requires a new definition [82], i.e. the first Riemann sheet for all quadrants but the second where the function is defined in the second Riemann sheet:

$$\ln^-(z_R + iz_I, z_0 - i0) = \ln(z_R + iz_I) - 2i\pi\theta(-z_0)\theta(z_I).
 \tag{26}$$

⁷This was the conjecture of Peierls: a pole on the second sheet is to be identified with an unstable particle.

It is easily seen that, as far as Feynman diagrams are concerned, $\ln^-(z)$ and $\ln(z)$ coincide when the internal masses are made complex while Mandelstam invariants remain real.

The numerical evaluation of logarithms of complex quantities, when needed, is better performed by using

$$\ln x = x \mathbf{R}_c \left(\frac{1}{4} x^2, x \right), \quad \arctan x = x \mathbf{R}_c (1, 1 + x^2), \quad (27)$$

where \mathbf{R}_c is one of the Carlson elliptic integrals [83].

In the following sections we will analyze the presence of regularized ATs for bubbles, triangles, boxes etc. and study their impact on physical observables; it should be emphasised that the presence of ATs depends on the structure of denominators of specific Feynman diagrams⁸ but their numerical impact on the full amplitude also depends on numerators. In this regard, we are assuming that the singularity spectrum of the S-matrix is confined to the union of the singularity spectra of the Feynman integrals, and we proceed to construct the singularity spectra of the Feynman integrals. Therefore, the scattering amplitude appears as the sum of infinitely many diagrams of increasing complexity and each diagram in principle can be completely investigated. In principle there is no reason for the S-matrix to be the sum of the diagrams but we work under the assumption that the diagrams represent the local behavior of the amplitude and that the whole picture can be recovered by gluing together all these local behaviors. For an interpretation of the Landau singularities as macroscopic causality see Refs. [84, 85].

Furthermore, at the amplitude level, a given branch cut is generically shared by several integrals while the leading singularities receive contributions from a single integral⁹. An additional comment concerns the difference between the Feynman diagram approach and the S-matrix theory [88]. Feynman integrals can be analytically continued around a Landau singularity: as a consequence Feynman diagram integrals are clearly singular only on the Landau surfaces obtained from the so-called $+\alpha$ Landau equations [89]. In S-matrix theory there is, a-priori, no $i\varepsilon$ prescription (unless it is adopted as an additional postulate).

It should be emphasized that a complete numerical study of different processes falls outside the scope of this paper where we limited our analysis to the evaluation of the anomalous part of the amplitudes. Furthermore, we have not analyzed the impact of parton distribution functions but the general rule is that, given an amplitude (squared), increasing the number of integrations decreases the effect.

3. Bubble diagrams

The whole procedure can be understood in terms of a simple example, the generalized bubble integral,

$$\mathbf{B}_0(\alpha) = \int_0^1 dx \chi^{-\alpha}, \quad \chi = s x^2 + (m_2^2 - m_1^2 - s)x + m_1^2. \quad (28)$$

We introduce complex masses, $m_i^2 \rightarrow m_i^2 - i\Gamma_i m_i$, and derive

$$\chi = s(x - X)^2 + \Delta_2, \quad (29)$$

where we have introduced

$$X = \frac{1}{2} \left(1 + \frac{m_1^2 - m_2^2}{2} \right) - \frac{i}{2} \frac{\Gamma_-}{s}, \quad \Delta_2 = \lambda(s, m_1^2, m_2^2) - \Gamma_-^2 + 2i \left[\Gamma_+ s - \Gamma_- (m_1^2 - m_2^2) \right], \quad (30)$$

⁸Because the vertices are point interactions, singularities in any local QFT are generated only by propagators.

⁹For the most general scenario this is an assumption, see the discussion on equivalent diagrams in Refs. [86, 87].

\sqrt{s} [GeV]	Re $B_0(1)$	Im $B_0(1)$	Re Δ_2	Im Δ_2	Re X	Im X
80	$0.78746 \cdot 10^{-3}$	$0.34494 \cdot 10^{-5}$	$-0.59143 \cdot 10^{-1}$	$0.22827 \cdot 10^{-3}$	1.2734	$-0.7031 \cdot 10^{-3}$
$\sqrt{s_*}$	$0.99996 \cdot 10^{-3}$	$0.54997 \cdot 10^{-5}$	0	0	1.1111	$-0.5556 \cdot 10^{-3}$
90	$0.99996 \cdot 10^{-3}$	$0.54998 \cdot 10^{-5}$	$0.30864 \cdot 10^{-6}$	$-0.16975 \cdot 10^{-8}$	1.1111	$-0.5556 \cdot 10^{-3}$
100	$0.15225 \cdot 10^{-2}$	$0.13213 \cdot 10^{-4}$	$0.99752 \cdot 10^{-2}$	$-0.10450 \cdot 10^{-3}$	0.9950	$-0.4500 \cdot 10^{-3}$
110	$0.13984 \cdot 10^{-1}$	$0.14968 \cdot 10^{-1}$	$0.13831 \cdot 10^{-6}$	$-0.15026 \cdot 10^{-3}$	0.9091	$-0.3719 \cdot 10^{-3}$
120	$-0.72742 \cdot 10^{-3}$	$0.16493 \cdot 10^{-2}$	$-0.17470 \cdot 10^{-1}$	$-0.16710 \cdot 10^{-3}$	0.8438	$-0.3125 \cdot 10^{-3}$

Table 1: Peierls zeros for a generalized two-point function.

where $\Gamma_{\pm} = \Gamma_1 m_1 \pm \Gamma_2 m_2$ and where λ is the Källén lambda function. With real masses the integral is singular when $0 < X < 1$ and $\lambda = 0$, i.e. $s = (m_1 \pm m_2)^2$ which are the so-called normal and pseudo threshold. We obtain

$$B_0(\alpha) = \frac{\Gamma(\alpha - 1/2)}{\Gamma(\alpha)} \left(\frac{\pi}{s}\right)^{1/2} \Delta_2^{1/2-\alpha} + \text{reg. terms}, \quad (31)$$

where Γ is the Euler gamma function. Furthermore, at the normal threshold (the leading Landau singularity for the bubble) the condition $0 < X < 1$ is always satisfied. With complex masses there is no singularity but for

$$s = \frac{\Gamma_1 m_1 - \Gamma_2 m_2}{\Gamma_1 m_1 + \Gamma_2 m_2} (m_1^2 - m_2^2), \quad (32)$$

we have the Peierls zero (Re $\Delta_2 = \text{Im } \Delta_2 = 0$) if

$$4m_1^2 m_2^2 (m_1^2 - m_2^2) (\Gamma_2^2 - \Gamma_1^2) = (m_1^2 \Gamma_1^2 - m_2^2 \Gamma_2^2)^2. \quad (33)$$

To show the numerical effect we select $m_1 = 100 \text{ GeV}$, $m_2 = 10 \text{ GeV}$ and $\Gamma_1 = 100 \text{ MeV}$. Deriving Γ_2 and $s = s_*$ from Eq.(33) we find $\sqrt{s_{PT}} - \sqrt{s_*} = 112.5 \text{ MeV}$, where the pseudo-threshold is at 90 GeV . Numerical results are shown in Tab. 1 where it can be seen that Im X is always negative, Re X decreases with s (but Re $X > 1$ at the pseudo-threshold), there is a cusp at the normal threshold and no special enhancement at $\sqrt{s_*}$.

4. Triangle diagrams

Consider the diagram of Figure 3 where the three external lines are off-shell, e.g. $H^* \rightarrow W^* W^*$. We must have

$$s \geq (M_1 + M_2)^2. \quad (34)$$

From the Kershaw theorem [42] we see that the physical-region Landau curve has six branches in the Q, q_1, q_2 space, i.e.

$$s > (m_1 + m_3)^2, \quad M_2^2 > (m_2 + m_3)^2, \quad M_1^2 < (m_1 - m_2)^2, \quad (35)$$

with $Q^0 > 0$ and $q_2^0 > 0$. The other branches are obtained by cyclic permutations and by the overall reflection of the external momenta. Our example will be as follows: there is an off-shell H with momentum Q going to off-shell Ws; internal lines are t, b quarks, i.e.

$$m_1 = m_3 = m_t, \quad m_2 = m_b. \quad (36)$$

Furthermore, $M_2 > m_t + m_b$ and $M_1 < m_t - m_b$. In this configuration, when the t-width is neglected, we obtain $X_{1,2}$, Gram and Cayley determinants,

$$G_3 = -\frac{1}{4} M_2^2 + \frac{1}{2} (s + M_1^2) - \frac{1}{4} (s - M_1^2)^2,$$

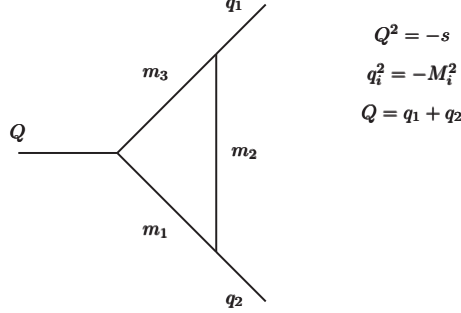


Figure 3: Triangle diagram: the general case with arbitrary internal and external masses.

$$\begin{aligned}
C_3 &= -\frac{1}{4} m_t^2 M_2^4 + \frac{1}{4} [s(m_t^2 + m_b^2 - M_1^2) + 2m_t^2 M_1^2] \\
&\quad - \frac{1}{4} s(m_t^2 - m_b^2)^2 + \frac{1}{4} s M_1^2 (m_t^2 + m_b^2) - \frac{1}{4} (m_t^2 M_1^4 + m_b^2 s^2), \\
G_3 X_1 &= \frac{1}{4} (s + M_1^2 + m_t^2 - m_b^2) M_2^2 - \frac{1}{4} (s - m_t^2 + m_b^2) s - \frac{1}{4} (M_1^2 + m_t^2 - m_b^2) M_1^2 + \frac{1}{2} s M_1^2, \\
G_3 X_2 &= \frac{1}{4} (M_1^2 + m_t^2 - m_b^2) M_2^2 + \frac{1}{4} (M_1^2 - m_t^2 + m_b^2) s - \frac{1}{4} (M_1^2 + m_t^2 - m_b^2) M_1^2,
\end{aligned} \tag{37}$$

The condition $\Delta_3 = 0$, at $\Gamma_t = 0$, can be seen as a quadratic equation in M_2^2 for fixed s and M_1 . Therefore, we require

$$\begin{aligned}
[T_1] \quad & \Delta_3 = 0, \\
[T_2] \quad & 0 < X_2 < X_1 < 1, \\
[T_3] \quad & s > (M_1 + M_2)^2.
\end{aligned} \tag{38}$$

The space-time picture is the following: the state of momentum Q decays into a $t\bar{t}$ pair, one of the top quarks decays into Wb , the b quark rescatters against the second t quark to produce a state with invariant mass M_2 . The solution of $\Delta_3 = 0$ can give complex M_2^2 , M_2^2 , real but negative, a real solution which does not satisfy condition $[T_2]$ in Eq.(38), a real solution satisfying $[T_2]$ (the X test) but not $[T_3]$ (singularity inside the physical region) and, finally, a physical singularity satisfying both $[T_2]$ and $[T_3]$. The distribution of physical-region singularities ($\Gamma_t = 0$) is shown in Figure 4 in the $\sqrt{s}-M_1$ plane with $350 \text{ GeV} < \sqrt{s} < 750 \text{ GeV}$ and $M_{1,2} > 10 \text{ GeV}$.

To study the corresponding Peierls zeros we introduce $s_{\pm} = M_1^2 \pm M_2^2$ and derive that

$$s_{+} = \frac{s_{-}^2}{s} + 2(m_t^2 - m_b^2), \quad s_{-}^2 = \frac{s}{2} \left\{ s - 4m_t^2 + 8m_b^2 \pm \left[(s - 4m_t^2)^2 + 16\Gamma_t^2 m_t^2 \right]^{1/2} \right\} \tag{39}$$

satisfy $\text{Re } \Delta_3 = \text{Im } \Delta_3 = 0$. Neglecting the b width and using the leading-order (LO) value for Γ_t we find no Peierls zeros inside the physical region defined by $s > (M_1 + M_2)^2$. For instance, for $\sqrt{s} = 350 \text{ GeV}$, the zero corresponds to invariant masses of 486.3 GeV and 254.0 GeV or to a negative value for s_{-}^2 .

We give an example in Figure 5 where we plot $L(sC_0)$ as a function of M_2 for $\sqrt{s} = 350 \text{ GeV}$, $M_1 = 120 \text{ GeV}$ and where the log-modulus function [74] is

$$L(x) = \text{sign}(x) \frac{\ln(1 + |x|)}{\ln 10}. \tag{40}$$

The effect of the normal threshold, $M_2 = m_t + m_b$, and of the anomalous threshold, $M_2 = 201.89 \text{ GeV}$ are clearly visible in the real part (solid line) and in the imaginary one (dashed line). Red curves correspond to the choice of $\Gamma_t/100$.

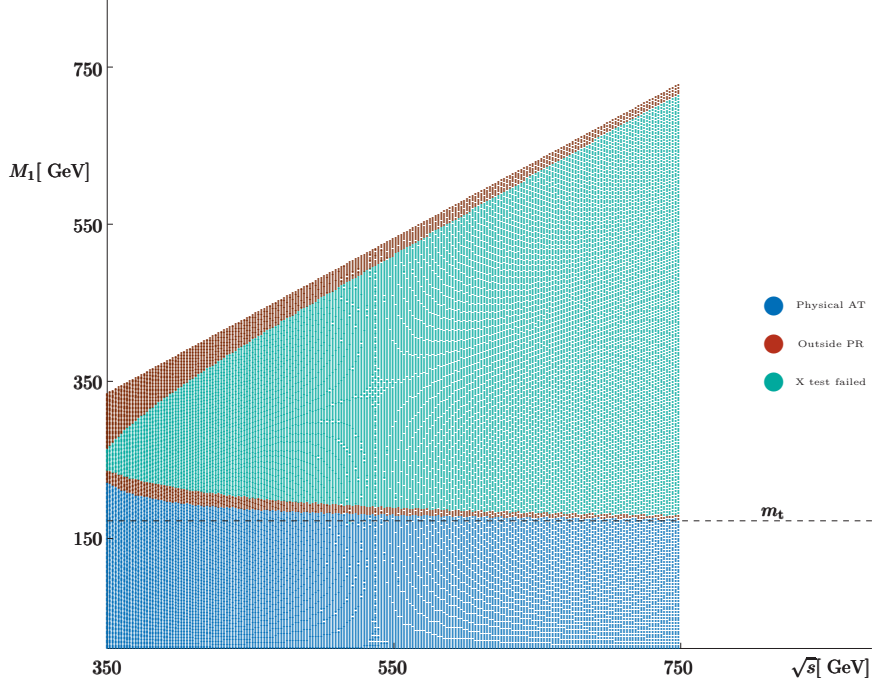


Figure 4: Physical and non physical AT for the triangle diagram of Figure 3 with internal masses given in Eq.(36). Here $350 \text{ GeV} < \sqrt{s} < 750 \text{ GeV}$ and $M_{1,2} > 10 \text{ GeV}$. For given values of \sqrt{s} and M_1 the value of M_2 corresponding to the AT is computed.

The M_2 distribution is also shown in Figure 6 for $\sqrt{s} = 350 \text{ GeV}$ and different values of M_1 . It can be seen that higher values for M_1 produce lower values for the AT.

In order to understand the impact of the AT on some realistic distribution we introduce the W complex pole, $s_w = \mu_w^2 - i\mu_w \gamma_w$ and define

$$C_\Delta(M_1) = s^4 \Delta_w(M_1) \int_{M_c}^{(\sqrt{s}-M_1)^2} dM_2^2 \Delta_w(M_2) \text{Re} C_0(s, M_1^2, M_2^2; m_t, m_b, m_t), \quad (41)$$

where the propagator factor is

$$\Delta_w(M) = \frac{1}{|M^2 - s_w|^2}, \quad (42)$$

and where M_c is a lower cut on M_2 . We show $L(C_\Delta)$ (Eq.(40)) in Figure 7 for 3 values of \sqrt{s} .

In order to understand the behavior of different curves in Figure 7 we recall that the occurrence of the AT requires $\sqrt{s} > 2m_t$, therefore there is no AT for $\sqrt{s} = 340 \text{ GeV}$. Furthermore we must have $M_1 > m_t + m_b$ and $M_2 < m_t - m_b$ or $M_1 < m_t - m_b$ and $M_2 > m_t + m_b$, with $M_1 + M_2 < \sqrt{s}$. The equation $\Delta_3 = 0$ is quadratic in M_2 and can be solved for fixed \sqrt{s}, M_1 and the solutions must satisfy conditions $T_{2,3}$ in Eq.(38). We find that at most one of the two solutions does it, as expected. In particular, for $\sqrt{s} = 350 \text{ GeV}$ we always find one real value for M_2 that corresponds to the AT if $M_1 < 168 \text{ GeV}$; M_2 is complex for $168 \text{ GeV} < M_1 < 177 \text{ GeV}$ with tiny imaginary part; M_2 is again real for $177 \text{ GeV} < M_1 < 226 \text{ GeV}$ and becomes imaginary for $M_1 > 226 \text{ GeV}$.

Finally, we consider the process $gg \rightarrow e^- \mu^+ \bar{\nu}_e \nu_\mu$, in particular the $gg \rightarrow H \rightarrow e^- \mu^+ \bar{\nu}_e \nu_\mu$ component. The question of gauge invariance has been discussed at length in Ref. [90]: given the process $gg \rightarrow F$, where F is an arbitrary final

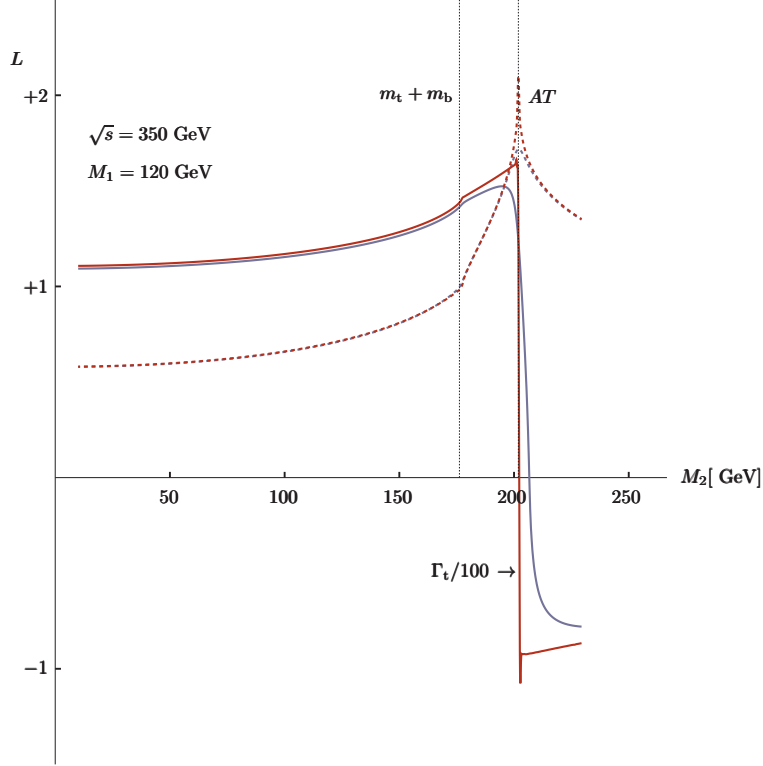


Figure 5: The log-modulus transformation of sC_0 as a function of M_2 for $\sqrt{s} = 350 \text{ GeV}$, $M_1 = 120 \text{ GeV}$. The red curves correspond to $\Gamma_t/100$.

state we want to separate the H component as

$$\sigma_{\text{gg} \rightarrow \text{H} \rightarrow \text{F}}(s) = \frac{1}{\pi} \sigma_{\text{gg} \rightarrow \text{H}} s^2 \Delta_{\text{H}}(s) \frac{\Gamma_{\text{H} \rightarrow \text{F}}}{\sqrt{s}}. \quad (43)$$

where s_{H} is the Higgs complex pole. To summarize: we would like to use the Higgs propagator with its complex pole with production and decay computed at arbitrary Higgs virtuality and not at the complex pole. As far as LO production is concerned, e.g. the ggH one-loop fermion triangle, there is never an issue of gauge-parameter dependence in going off-shell; in this respect higher order QCD corrections are not a problem.

Consider now the decay, i.e. $\Gamma(\text{H} \rightarrow \text{F})$ in Eq.(43): the amplitude $A(\text{H} \rightarrow \text{F})$, for each final state and as long as we include the complete set of diagrams at one-loop order, is gauge-parameter independent if the Higgs boson is on its mass-shell. However, as soon as we put an external leg off-shell, the amplitude must be coupled to the corresponding physical source and only the complete process $\text{I} \rightarrow \text{F}$ is gauge-parameter independent. The latter does not exclude the existence of subsets of diagrams that satisfy the requirement but this can only be examined on a case-by-case basis. To rephrase it, if the Higgs boson is off shell, the matrix element still respects gauge invariance (in most cases) in LO and in next-to-leading (NLO) QCD but in NLO EW gauge invariance is lost. How to deal with this situation? Technically speaking, we have a matrix element

$$\Gamma(\text{H} \rightarrow \text{F}) = f(s, \mu_{\text{H}}^2), \quad (44)$$

where s is the virtuality of the external Higgs boson, μ_{H} is the mass of internal Higgs lines and Higgs wave-function renormalization has been included. The following happens: $f(s_{\text{H}}, s_{\text{H}})$ is gauge-parameter independent to all orders while $f(\mu_{\text{H}}^2, \mu_{\text{H}}^2)$ is gauge-parameter independent at one-loop but not beyond, $f(s, \mu_{\text{H}}^2)$ is not. In order to account for the off-shellness of the Higgs boson we defined a viable scheme by choosing (at one loop level) $f(s, s)$, i.e. we intuitively replace the on-shell decay of the Higgs boson of mass μ_{H} with the *on-shell* decay of an Higgs boson of

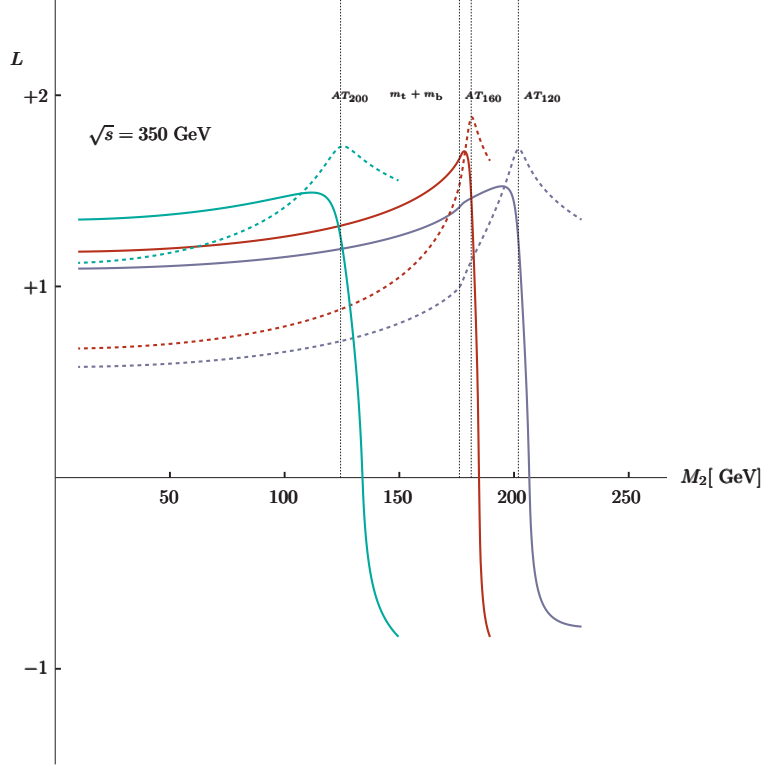


Figure 6: The log-modulus transformation of sC_0 as a function of M_2 for $\sqrt{s} = 350 \text{ GeV}$, and $M_1 = 120 \text{ GeV}$ (blue), $M_1 = 160 \text{ GeV}$ (red) and $M_1 = 200 \text{ GeV}$ (emerald). Solid curves give the real part while dashed curves give the imaginary part.

mass \sqrt{s} and not with the off-shell decay of an Higgs boson of mass μ_H . The same applies for the NLO EW correction to production.

In our case we are interested in the effect of the AT present in the triangle graph HWW with internal quark lines and, therefore, there is no problem in the off-shellness of the process (there are no internal Higgs lines); furthermore, no other diagram produces an AT (at the same location). As a consequence we can analyze $H \rightarrow e^- \mu^+ \bar{\nu}_e \nu_\mu$ with off-shell H and look for the impact of the AT on $\Gamma(H \rightarrow e^- \mu^+ \bar{\nu}_e \nu_\mu)$. The process is now

$$H(Q) \rightarrow W^+(q_1 + q_2) + W^-(q_3 + q_4) \rightarrow \nu_\mu(q_1) + \mu^+(q_2) + e^-(q_3) + \bar{\nu}_e(q_4), \quad (45)$$

with $Q^2 = -s$ and light fermion masses are neglected. The full process is given in terms of s and 5 additional Mandelstam invariants [91],

$$\begin{aligned} s_1 &= -(q_2 + q_3 + q_4)^2, & s_2 &= -(q_3 + q_4)^2, \\ u_1 &= -(q_1 + q_3 + q_4)^2, & u_2 &= -(q_1 + q_2 + q_4)^2, \\ t_2 &= -(q_1 + q_4)^2. \end{aligned} \quad (46)$$

Next we define $s_2 = M^2$ and study the $d\Gamma/dM$ distribution,

$$\frac{d\Gamma}{dM} = \frac{d\Gamma}{dM}\Big|_{\text{LO}} + \frac{d\Gamma}{dM}\Big|_{\text{NLO,AT}} + \frac{d\Gamma}{dM}\Big|_{\text{NLO,rest}}. \quad (47)$$

Since our interest is, in the first place, on the AT effect we limit the calculation to δ_{AT} , the percentage correction introduced by the AT.

Results are shown in Figure 8 for different values of \sqrt{s} . To understand the behavior of radiative corrections two effects should be taken into account: M_1 is non resonant if $M_2 > \sqrt{s} - M_W$ and above a certain value for M_2 there is

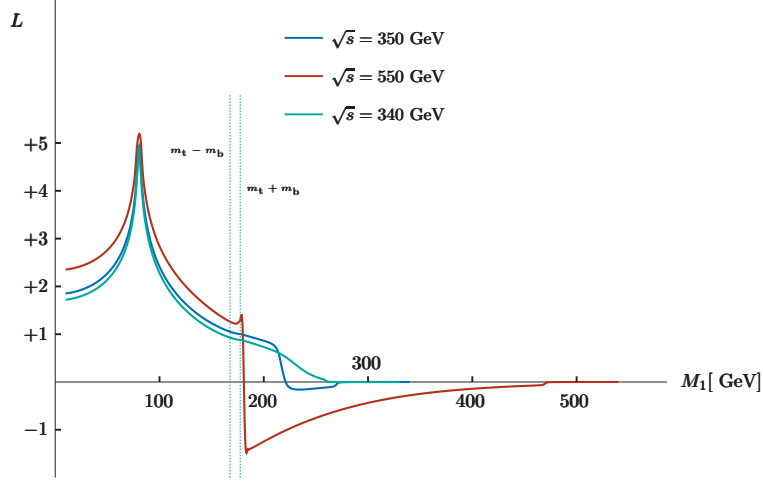


Figure 7: $L(C_\Delta)$ as a function of M_1 for different values of \sqrt{s} . C_Δ is defined in Eq.(41) and $L(x)$ in Eq.(40).

no AT corresponding to a real value of M_1 . For instance, for $\sqrt{s} = 350 \text{ GeV}$ this happens above $M_2 \approx 226 \text{ GeV}$. The (blue) dashed line corresponds to $\sqrt{s} = 350 \text{ GeV}$ and $\Gamma_t \rightarrow \Gamma_t/100$, showing the effect of the AT.

4.1. AT induced by QCD/QED radiation

It is easy to see that there is no AT for $X \rightarrow \bar{f}f$, where X can be an on-shell BSM Higgs boson, the off-shell SM Higgs boson or an off-shell Z boson. However, considering the processes

$$X \rightarrow \bar{b}bg, \quad X \rightarrow \bar{f}f\gamma, \quad (48)$$

we find a class of one-loop diagrams (a representative is a) in Figure 9) which admit a physical-region AT. The processes shown in Eq.(48) present several important features, as discussed in Refs. [92, 93]: if X is a Higgs boson the tree-level coupling $H-\bar{f}-f$ is Yukawa suppressed, i.e. proportional to m_f . This property is preserved in higher loops; however this is not the case when a photon (gluon) is emitted and, already at one loop, there are contributions surviving the $m_f \rightarrow 0$ limit. We assume that the BSM (heavy) Higgs boson has couplings proportional to the SM ones; for instance, in the singlet extension of the SM the HWW , $H\phi\phi$ and $H\bar{f}f$ couplings are equal to the corresponding SM couplings times $\sin\alpha$ where α is the mixing angle between the (SM) doublet and the singlet.

$\bar{b}bg(g)$ final state.

If s denotes the X virtuality, we find a small window between $\sqrt{s} = 345.5 \text{ GeV}$ where the AT corresponds to $M(\bar{b}g) = 264.81 \text{ GeV}$ and $\sqrt{s} = 370 \text{ GeV}$ where the AT corresponds to $M(\bar{b}g) = 252.90 \text{ GeV}$. Diagram c) in Figure 9 is the representative of a class not supporting a (physical-region) LLS, i.e. the leading singularity of diagram a) in Figure 9 is only subleading for diagram c), corresponding to the contraction of an internal top line.

Consider now the process $X \rightarrow \bar{b}bgg$, the double gluon emission (e.g. diagram b) in Figure 9). Also in this case there is a physical-region AT as illustrated in Figure 10 where we show $M(\bar{b}g)$ as a function of $M(\bar{b}g)$ at the AT; as expected, one of the invariant masses should be above $m_t + M_W$ with the other below $m_t - M_W$. It is worth noting that even in this case there is only a small window above $\sqrt{s} = 2m_t$ where the AT shows up, as illustrated by the red curve in Figure 10 which corresponds to 360 GeV . The physical-region AT disappears around $\sqrt{s} = 370 \text{ GeV}$.

However, above 370 GeV Peierls zeros start to appear, e.g. at $\sqrt{s} = 370 \text{ GeV}$ the zero corresponds to one invariant mass of 110.36 GeV with the other at 200.25 GeV . At $\sqrt{s} = 512 \text{ GeV}$ the values are 9.73 GeV and 245.63 GeV ; above this value the two invariant masses are outside the physical region.

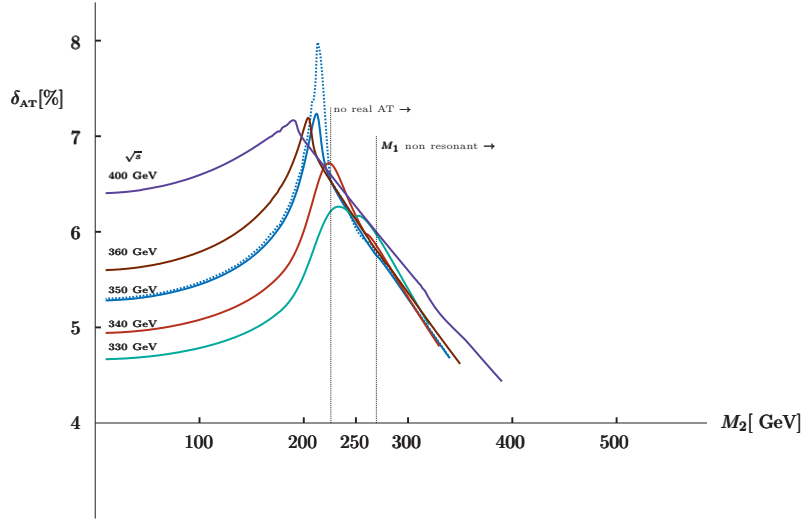


Figure 8: Percentage radiative corrections around the AT (Eq.(47)) for the process of Eq.(45).

The same line of argument applies to other processes, e.g. $gg \rightarrow \bar{b}bg$ and $gg \rightarrow \bar{b}bgg$ (also to a $\bar{q}q$ initial state). Let us consider $H^* \rightarrow \bar{b}bg$ with an off-shell Higgs boson: we find the following pattern for the amplitude,

$$A_{\text{LO}} = A_{\text{LO}}^{(1)} m_b + \mathcal{O}(m_b^2), \quad A_{\text{NLO}} = A_{\text{NLO}}^{(0)} + A_{\text{NLO}}^{(1)} m_b + \mathcal{O}(m_b^2). \quad (49)$$

Therefore, $|A|^2$ is $\mathcal{O}(m_b^2)$ at LO; there is no interference between $A_{\text{LO}}^{(1)}$ and $A_{\text{NLO}}^{(0)}$ so that the interference (NLO) is also $\mathcal{O}(m_b^2)$. Since A_{NLO} contains $A_{\text{NLO}}^{\text{AT}}$ we can include an additional (NNLO) term given by the square of $A_{\text{NLO}}^{(0)}$. Taking into account the logarithmic nature of the AT, the suppression factor $1/(16\pi^2)$ for the loop and the value of the b-quark mass we do not find any significant effect due to the AT. The process $H^*(P) \rightarrow b(q_1) + \bar{b}(q_2) + g(q_3)$, with $P^2 = -s$ is described by two invariants,

$$s_1 = -(P - q_1)^2, \quad u_1 = -(P - q_2)^2, \quad (50)$$

with the following boundaries

$$m_b^2 \leq s_1 \leq (\sqrt{s} - m_b)^2, \quad u_{1-} \leq u_1 \leq u_{1+}, \quad (51)$$

where the limits for u_1 are

$$u_{1\pm} = s + m_b^2 - \frac{1}{2s_1} (s_1 + m_b^2)(s + s_1 - m_b^2) \pm \frac{1}{2s_1} \lambda^{1/2}(s_1, m_b^2, 0) \lambda^{1/2}(s, s_1, m_b^2). \quad (52)$$

After inserting the relevant parts of the one-loop corrections we obtain the percentage AT corrections to the pseudo-observable $d\Gamma(H^* \rightarrow \bar{b}bg)/dM(bg)$, i.e. $\delta_{\text{NLO,NNLO}}^{\text{AT}}$. For $\sqrt{s} = 350 \text{ GeV}$ the AT is at $\sqrt{s_1} = M(bg) \approx 257.82 \text{ GeV}$. After imposing a cut of 10 GeV on all final state invariant masses we obtain the result shown in the left panel of Figure 11; NLO and NNLO are indistinguishable. The AT effect is very small and corresponds to a change in the curvature of δ^{AT} .

$e^+e^- \gamma$ final state.

For this process we can have a $W-v-W$ triangle: in this case \sqrt{s} must be above $2M_W$ for a physical-region AT, as dictated by the Coleman-Norton theorem. The physical-region AT starts at $\sqrt{s} = 161.05 \text{ GeV}$ with $M(e^+\gamma) = 110.64 \text{ GeV}$ and approaches $M(e^+\gamma) = M_W$ for very large values of \sqrt{s} . It is worth noting that all diagrams contributing to $H^* \rightarrow Z(\rightarrow e^+e^-) + \gamma$ do not show an AT. For this process, due to the small value of m_e the inclusion of NNLO terms changes drastically the result as shown in the right panel of Figure 11, i.e. the NNLO contribution is six orders of

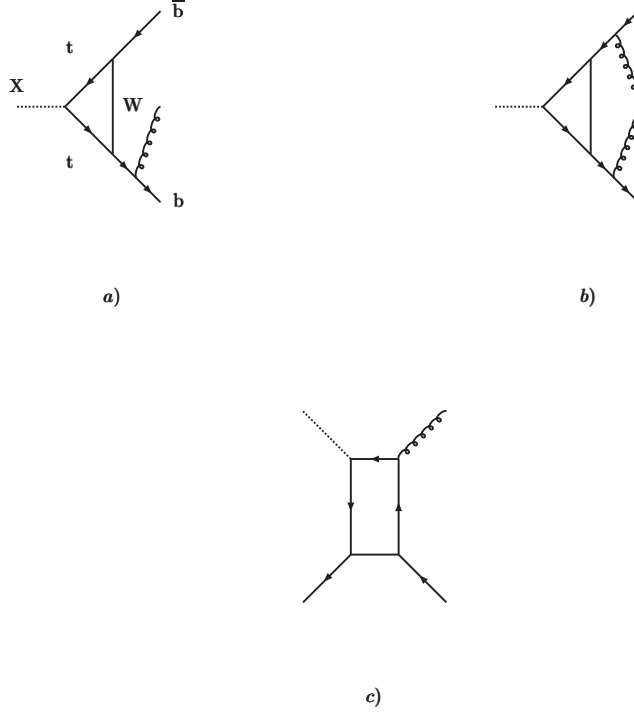


Figure 9: Example of diagrams contributing to $X \rightarrow \bar{b}b g$ and $X \rightarrow \bar{b}b g g$.

magnitude larger than the LO term at $\sqrt{s} = 170 \text{ GeV}$. Here the red curve corresponds to no cut while the red one corresponds to a cut of 10 GeV on all final state invariant masses. In this case δ^{AT} shows a peak at the AT.

We can also have a Z - e - Z triangle: in this case \sqrt{s} must be above $2M_Z$. The physical-region AT starts at $\sqrt{s} = 182.38 \text{ GeV}$ with $M(e^+\gamma) = 128.96 \text{ GeV}$ and approaches $M(e^+\gamma) = M_Z$ for very large values of \sqrt{s} .

e^+e^- colliders.

It is worth noting that the same qualitative behavior will be found for

$$e^+ + e^- \rightarrow Z/\gamma \rightarrow \bar{b} + b + g, \quad e^+ + e^- \rightarrow Z/\gamma \rightarrow \bar{f} + f + \gamma, \quad (53)$$

and also for $e^+ + e^- \rightarrow \bar{b} + b + \gamma + \gamma$, an irreducible background process in measuring the $H \rightarrow \gamma\gamma$ decay at a linear collider.

5. Box diagrams

Consider the diagram of Figure 12 where $Q = q_1 + q_2 + q_3$, with $Q^2 = -s$ and $q_i^2 = -M_i^2$. The physical region is defined in terms of invariants [91],

$$s_1 = -(Q - q_1)^2, \quad u_1 = -(Q - q_2)^2. \quad (54)$$

We derive

$$(M_2 + M_3)^2 \leq s_1 \leq (\sqrt{s} - M_1)^2, \quad u_{1-} \leq u_1 \leq u_{1+}, \quad (55)$$

where the limits for u_1 are

$$u_{1\pm} = s + M_2^2 - \frac{1}{2s_1} \left[(s_1 + M_2^2 - M_3^2)(s + s_1 - M_1^2) \mp \lambda^{1/2}(s_1, M_2^2, M_3^2) \lambda^{1/2}(s, s_1, M_1^2) \right]. \quad (56)$$

Therefore, we are interested in the process $gg \rightarrow \bar{b}bH$ where H can be an off-shell Higgs boson of the SM or some, on-shell, heavy Higgs boson present in some BSM model. Another case of interest is represented by $gg \rightarrow \bar{b}bHH$;

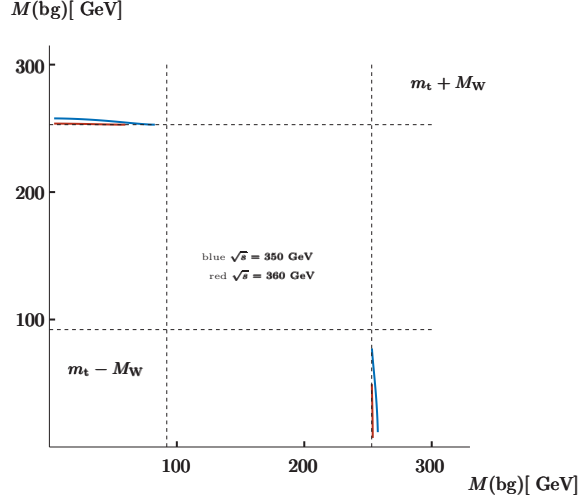


Figure 10: Anomalous threshold in $X \rightarrow \bar{b}b g g$.

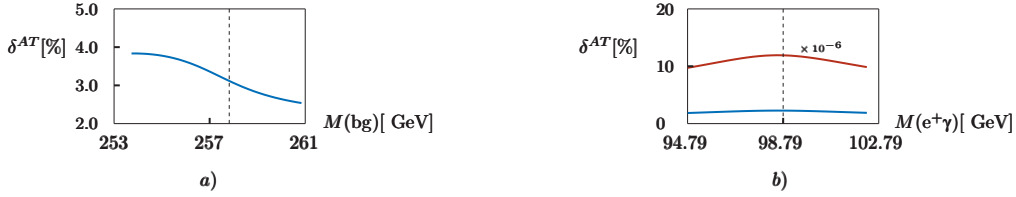


Figure 11: AT induced radiative corrections for a) $H^* \rightarrow \bar{b}b g$ and b) $H^* \rightarrow e^+e^- \gamma$. The H virtuality is a) $\sqrt{s} = 350 \text{ GeV}$ and b) $\sqrt{s} = 170 \text{ GeV}$.

here the two SM Higgs bosons are on shell, therefore $q_2 = q_{21} + q_{22}$ with $q_{2i}^2 = -M_H^2$ and M_2 is the invariant mass of the HH pair. Using $M_{1,3} = m_b$ and $M = M_2$ we compute the corresponding Δ_4 using $L_4 = m_t^2$ and

$$G_4 = -\frac{1}{4} (aM^4 + bM^2 + c), \quad (57)$$

$$a = m_b^2, \quad b = (s - s_1)u_1 - (2s + u_1)m_b^2, \quad c = (s_1 + u_1 - s)s_1 u_1 + (s^2 - s u_1 - 2s_1 u_1)m_b^2 + u_1 m_b^4. \quad (58)$$

It can be seen that $\Delta_4 = 0$ produces a quadratic equation in M^2 that can be solved for fixed s, s_1, u_1 . A scan in the $s_1 - u_1$ plane is shown in Figure 13 for $\sqrt{s} = 350 \text{ GeV}$; the blue region shows values for M^2 which correspond to a physical-region AT, i.e. $\Delta_4 = 0$, ordered values for X_i ($0 < X_3 < X_2 < X_1 < 1$) and a real value for M inside the physical region given in Eq.(55).

Next we introduce complex poles for W and t and look for Peierls zeros. The two equations, $\text{Re } \Delta_4 = 0$ and $\text{Im } \Delta_4 = 0$ are quadratic in u_1 and M^2 for fixed s and s_1 generating four solutions. To give an example we fix $\sqrt{s} = 350 \text{ GeV}$ and derive

$\Gamma = 0$ one of the solutions for a physical-region AT is $\sqrt{s_1} = 259.15 \text{ GeV}$, $\sqrt{u_1} = 38.05 \text{ GeV}$ and $M = 162.46 \text{ GeV}$

$\Gamma \neq 0$ for $\sqrt{s_1} = 259.15 \text{ GeV}$, one solution returns a negative value for u_1 and the other three (two are coincident) return $M = 172.87 \text{ GeV}$, $\sqrt{u_1} = 58.13 \text{ GeV}$ and $M = 191.84 \text{ GeV}$, $\sqrt{u_1} = 158.16 \text{ GeV}$, both outside the physical region.

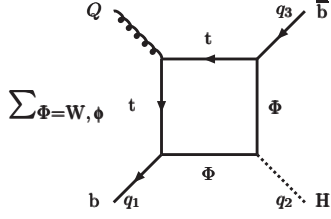


Figure 12: Family a) for $g(Q) \rightarrow b(q_1) + \bar{b}(q_3) + H(q_2)$.

Any box diagram is decomposed into a box in 6 dimensions and four triangles: an example is given in Figure 14. As a consequence we have to look not only for the LLS of the box but also for the subleading ones, which are the leading singularities for the triangles.

Old examples can be found in Ref. [40] for the process $\bar{p}p \rightarrow KK\pi\pi$ where peaks were predicted for the amplitude squared in a certain range of the external variables.

We start our analysis by looking at $g(Q) \rightarrow b(q_1) + \bar{b}(q_3) + X(q_2)$ at the point

$$P = \{\sqrt{s} = 350 \text{ GeV} ; \sqrt{s_1} = 259.15 \text{ GeV} ; \sqrt{u_1} = 155.20 \text{ GeV}\}, \quad (59)$$

as a function of $M^2 = -q_2^2$. It is worth noting that the location of the AT does not depend on the nature of X, but its numerical impact on the amplitude does.

For zero widths there is a physical-region AT at $M = 187.72 \text{ GeV}$; the Peierls zeros corresponding to $\sqrt{s_1} = 259.15 \text{ GeV}$ are located at $\sqrt{u_1} = 58.13 \text{ GeV}$, $M = 172.87 \text{ GeV}$ and $\sqrt{u_1} = 158.16 \text{ GeV}$, $M = 191.84 \text{ GeV}$. They are both outside the physical region with the latter close to the boundary $u_{1-} \leq u_1 \leq u_{1+}$.

In Figure 15 we plot $L(s^2 \text{Re } D_0)$ (Eq.(40)) corresponding to $g(Q) \rightarrow b(q_1) + \bar{b}(q_3) + X(q_2)$ at the point of Eq.(59). A blow up of the same figure is shown in Figure 16, including the imaginary part.

To understand the behavior of D_0 we split the function as follows: $V(x_1, x_2, x_3)$ is the quadratic form for the box; introduce triangles

$$T = \sum_{i=0}^3 (X_i - X_{i+1}) \int dS_2 V^{-1}(\widehat{ii+1}), \quad (60)$$

where $X_0 = 1$, $X_4 = 0$ and $(\widehat{01}) = (1, x_1, x_2)$ etc. are contractions. Therefore we obtain

$$D_0(\text{dim} = 4) = -\frac{1}{2\Delta_4} [D_0(\text{dim} = 6) - T] = -\frac{1}{2\Delta_4} \left\{ \frac{3}{2\Delta_4} [D_0(\text{dim} = 8) - \frac{1}{2}T] - T \right\}, \quad (61)$$

and plot

$$D_0(\text{dim} = 4), \quad D_0^{(6)}(\text{dim} = 4) = -\frac{1}{2\Delta_4} D_0(\text{dim} = 6), \quad D_0^{(8)}(\text{dim} = 4) = -\frac{3}{4\Delta_4^2} D_0(\text{dim} = 8), \quad (62)$$

where the $\text{dim} = 8$ part is

$$D_0(\text{dim} = 8) = \int dS_3 \left[\ln V(x_1, x_2, x_3) + \frac{2}{3} \right]. \quad (63)$$

The 3 components introduced in Eq.(62) are shown in Figure 17 for $g(Q) \rightarrow b(q_1) + \bar{b}(q_3) + X(q_2)$ at the point of Eq.(59).

Finally we introduce

$$I_{D_0} = \int_{u_{1-}}^{u_{1+}} du_1 \text{Re } D_0, \quad (64)$$

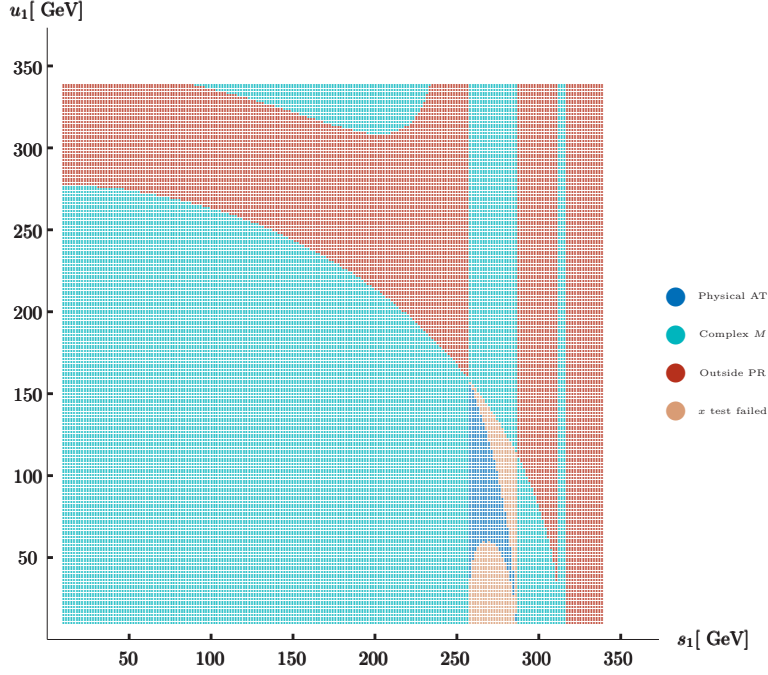


Figure 13: A scan in the $s_1 - u_1$ plane searching for a physical-region AT in $gg \rightarrow \bar{b}bH(HH)$.

where $u_{1\pm}$ are given in Eq.(56). The corresponding function $L(sI_{D_0})$ (Eq.(40)) is shown in Figure 18 as a function of M for three values of s_1 and $\sqrt{s} = 350 \text{ GeV}$. Here the D_0 -function correspond to $m_1 = m_4 = m_t$ and $m_2 = m_3 = M_W$. To show the impact of the AT we also plot (dashed blue line) the D_0 -function corresponding to $m_1 = m_4 = M_W$ and $m_2 = m_3 = m_t$, a configuration where the AT is absent.

More boxes.

Other examples involving box diagrams are $g + g(e^+ + e^-) \rightarrow W^+ + W^- + H$, with an on-shell Higgs boson and, at least, one off-shell W . Here $g + g \rightarrow g$ or $e^+ + e^- \rightarrow Z/\gamma$ with $g(Z/\gamma)$ attached to a box where the other external lines are WW and the Higgs boson (coupled to b internal lines).

5.1. Anomalous threshold and gauge invariance

Given the amplitude for a process supporting an anomalous threshold within the physical region we would like to split it into two components, i.e. $A_{AT} + A_{reg}$. In order to have a meaningful result we must discuss gauge invariance. Consider an off-shell gluon producing a $\bar{b}b$ pair and an heavy Higgs, e.g. the one in the singlet extension of the SM; the full process will be $g + g \rightarrow \bar{b} + b + H$. To discuss gauge invariance we work in the R_ξ -gauge where propagators are

$$W \rightarrow \frac{1}{p^2 + M_W^2} \left(\delta_{\mu\nu} + \frac{p_\mu p_\nu}{M_W^2} \right) - \frac{p_\mu p_\nu}{M_W^2 (p^2 + \xi^2 M_W^2)}, \quad \phi \rightarrow \frac{1}{p^2 + \xi^2 M_W^2}, \quad (65)$$

where ϕ is a Higgs-Kibble ghost. Consider the four diagrams, family a), shown in Figure 12: it is easy to show that the corresponding AT can be physical. Next we perform a “scalarization” of the amplitude which gives a collection of D_0 -functions, C_0 -functions and B_0 -functions.

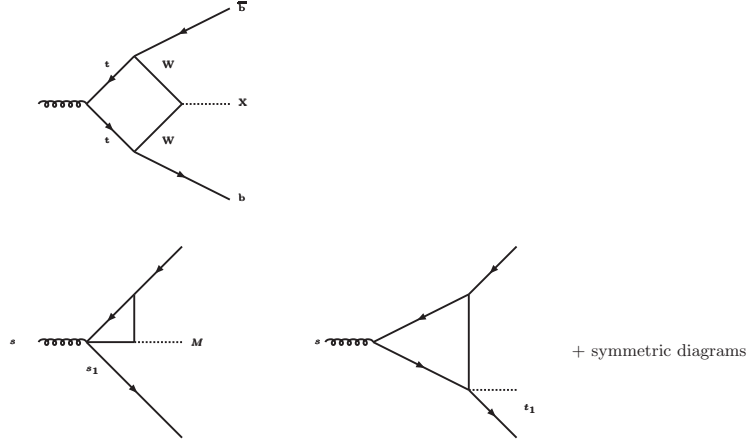


Figure 14: Box diagram producing an AT for $g \rightarrow \bar{b}bX$ where X can be some heavy BSM Higgs boson, an off-shell SM Higgs boson or a pair of two (on-shell) SM Higgs boson. In the second part of the figure we show two of the four triangles obtained by shrinking one line of the box to a point.

D_0 -approximation It is easy to see that the D_0 part of the amplitude is ξ -independent, i.e. D_0 -functions depending on $\xi^2 M_W^2$ cancel. Therefore we could define A_{AT} in terms of scalar boxes, including the rest in A_{reg} .

Minimal subset Alternatively, we can search for S_{AT} , the minimal subset of diagrams which is ξ -independent, satisfies Ward-Slavnov-Taylor identities (if applicable) and supports a physical-region AT. The corresponding procedure can be visualized as follows: scalarization produces triangles which are contractions of the original box, i.e. are obtained by shrinking one line of the box to a point; therefore, we must add family b), i.e. all boxes that give the same set of contractions (see Figure 19), and family c), i.e. all b - b -H (pure) triangles with a gluon coupled to b current.

5.1.1. Renormalization

As has been said many times our goal is not to perform the full calculation, therefore renormalization has to be understood in the \overline{MS} scheme with the renormalization scale set at the highest scale in the process under consideration.

5.1.2. π^2 enhancement

A C_0 -function is given by the integral

$$I = \int_0^1 dx_1 \int_0^{x_1} dx_2 \left[\sum_{i,j=1,2} (x_1 - X_i) H_{ij} (x_j - X_j) + \Delta_3 \right]^{-1}. \quad (66)$$

In general, in the complex mass scheme $\Delta_3, X_{1,2} \in \mathbb{C}$. There are configurations where $|\Delta_3| \ll 1$, although far from the AT, and where $|H_{11}| \ll 1$ (or $|H_{22}| \ll 1$) with $0 < \text{Re} X_2 < 1$ (or $0 < \text{Re} X_1 < 1$ but not both). The condition for H_{ij} is always satisfied when we have light external particles. Therefore, choosing the case $|H_{22}| \ll 1$, we can write

$$\begin{aligned} I &\approx \int_0^1 dx_1 \int_0^{x_1} dx_2 \left[H_{11} (x_1 - X_1)^2 + 2H_{12} (x_1 - X_1)(x_2 - X_2) \right]^{-1} \\ &= \frac{1}{2} H_{12}^{-1} \left\{ \left[\ln(2H_{12}(X_1 - X_2)) - \ln(-2H_{12}X_2) \right] \ln\left(1 - \frac{1}{X_1}\right) + \text{di-logarithms} \right\}. \end{aligned} \quad (67)$$

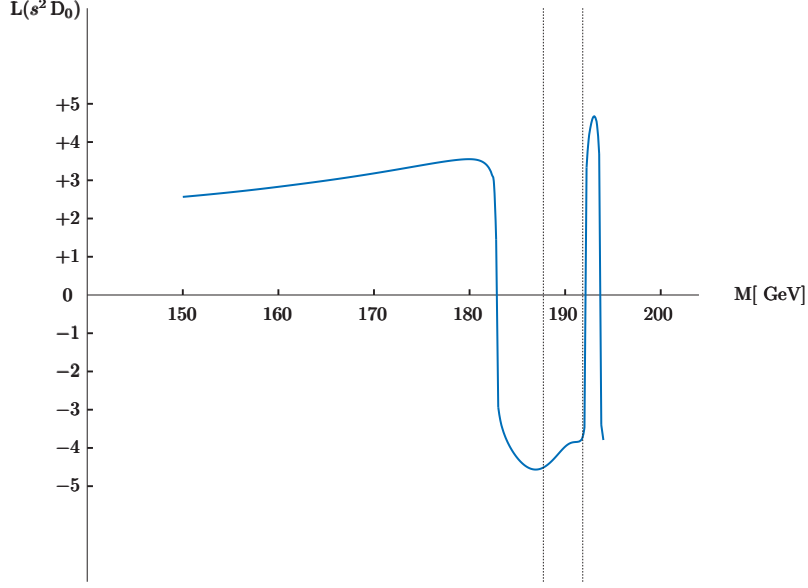


Figure 15: The real part of $s^2 D_0$ for $g(Q) \rightarrow b(q_1) + \bar{b}(q_3) + X(q_2)$ at the point of Eq.(59). $L(x)$ is defined in Eq.(40).

With $\text{Re}X_1 \in [0, 1]$ and $|\text{Im}X_1| \ll 1$ but $\text{Im}X_1 > 0$, we obtain

$$I \approx \frac{i\pi}{2} H_{12}^{-1} \text{Re} \left[\ln(2H_{12}(X_1 - X_2)) - \ln(-2H_{12}X_2) \right] + \text{rest}. \quad (68)$$

This C_0 -function will be part of the one-loop corrections to a given LO amplitude. Since A_{LO} is in general real this “ $i\pi$ ” term will not interfere but the NLO amplitude squared will receive a “ π^2 ” enhancement. As we will see in the following sections this is often the case, resulting in NNLO corrections (the NLO squared) which are much larger than the NLO ones. Clearly, only a complete calculation can decide the fate of these “ π^2 ” terms. Note that this enhancement should not be confused with the “pinch”, the latter requiring both X_1 and X_2 to be inside $[0, 1]$.

5.2. The process $g + g \rightarrow \bar{b} + b + X$

The full process to be studied will be

$$g(p_1) + g(p_2) \rightarrow b(q_1) + X(q_2) + \bar{b}(q_3), \quad (69)$$

requiring the following set of invariants:

$$s = -P^2 = -(p_1 + p_2)^2, \quad s_1 = -(P - q_1)^2, \quad u_1 = -(P - q_2)^2, \quad t_0 = -(p_1 - q_1)^2, \quad t_1 = -(p_1 - q_2)^2. \quad (70)$$

Here X is a scalar state of invariant mass M . Therefore it can represent some heavy BSM Higgs boson, a pair of SM Higgs boson ($gg \rightarrow \bar{b}bHH$), a pair of W bosons ($gg \rightarrow \bar{b}bW^+W^-$).

For real masses we observe that the region of phase space containing ATs becomes smaller and smaller when s increases and disappears for \sqrt{s} approximately greater than 438.5 GeV . This is not the case for Peierls zeros; we have analyzed those zeros which are inside the physical phase space and for which

$$0 < \text{Re} X_3 < \text{Re} X_2 < \text{Re} X_1 < 1. \quad (71)$$

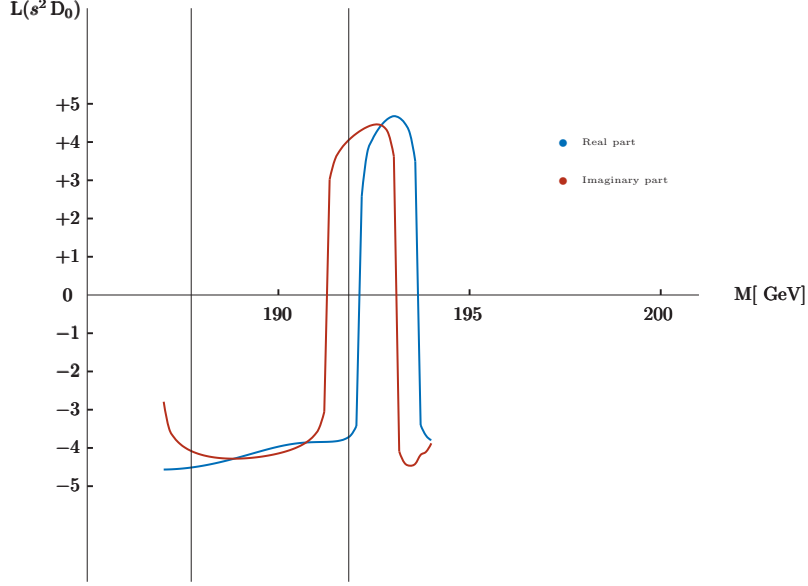


Figure 16: Blow up of Figure 15.

To give an example we consider $\sqrt{s} = 865 \text{ GeV}$ and $\sqrt{s_1} = 516.21 \text{ GeV}$. There are four solutions to $\Delta_4 = 0$ and one of them satisfies the requested conditions, corresponding to $M = 308.06 \text{ GeV}$ and $\sqrt{u_1} = 556.94 \text{ GeV}$ with

$$X_3 = 0.186 + i0.977 \cdot 10^{-3}, \quad X_2 = 0.250 - i0.171 \cdot 10^{-2}, \quad X_1 = 0.625 + i0.793 \cdot 10^{-3}. \quad (72)$$

The evaluation of loop integrals which are regular when the corresponding BST factor is zero requires an additional comment: when internal masses are real the solution has been described in Ref. [51]. For instance, consider the three-point function, characterized by a polynomial

$$V(x_1, x_2) - i0 = [V_0(x_1, x_2) - i0] + (\Delta_3 - i0). \quad (73)$$

In section 4.4.1. of Ref. [51] it is found that one can write

$$C_0 = \frac{1}{\Delta_3} \left[\int dS_2 \ln \frac{V}{V_0} - \frac{1}{2} \sum_{i=0}^2 (X_i - X_{i+1}) \int dS_1 \ln \frac{V(\widehat{ii+1})}{V_0(\widehat{ii+1})} \right]. \quad (74)$$

When complex masses are introduced the imaginary part of V has always the same sign, but this is not the case for V_0 ; furthermore, $\text{Im } V$ and $\text{Im } V_0$ have, in general, different signs so that one cannot reconstruct terms like $\ln(V/V_0)$ as done in Eq.(74). Therefore, we will write

$$V(x_1, x_2; \{\mathbf{I}\}) = V_0(x_1, x_2; \{\mathbf{I}\}) + \Delta_3(\{\mathbf{I}\}), \quad (75)$$

where $\{\mathbf{I}\}$ is the set of invariants describing the process. When

$$\Delta_3(\{\bar{\mathbf{I}}\}) = 0, \quad (76)$$

we will subtract, with a double BST algorithm, $V_0(x_1, x_2; \{\bar{\mathbf{I}}\})$ taking care of reconstructing $\ln(V/V_0)$ only when $|\Delta_3|$ is small enough and the imaginary parts of numerator and denominator have the same sign. Summarizing: let $\bar{X}_i = X_i(\{\bar{\mathbf{I}}\})$, we will use

$$\left[1 + \frac{1}{2(\mu+1)} (x-X)^t \partial_x \right] V^{\mu+1}(x_1, x_2; \{\mathbf{I}\}) = \Delta_3(\{\mathbf{I}\}) V^\mu(x_1, x_2; \{\mathbf{I}\}),$$

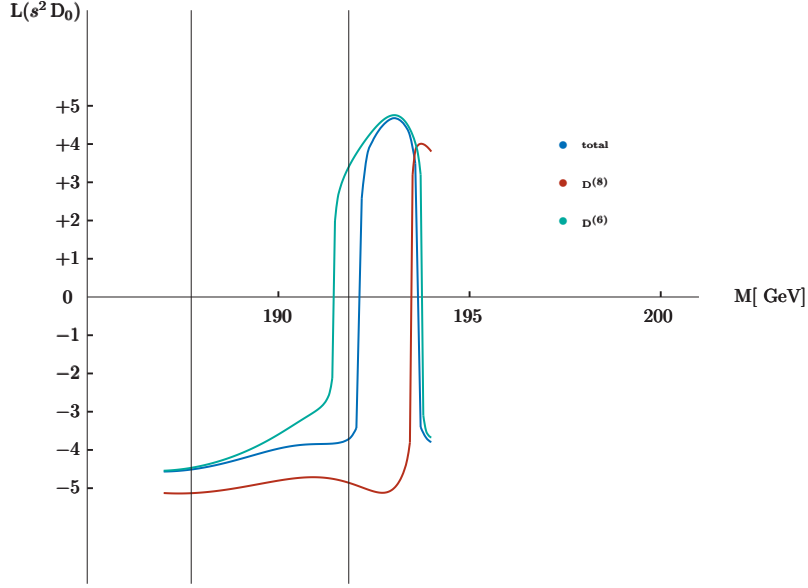


Figure 17: Different components for $\text{Re } D_0$ as explained in Eq.(62).

$$\left[1 + \frac{1}{2(\mu+1)}(x-\bar{X})^t \partial_x\right] \mathbf{V}_0^{\mu+1}(x_1, x_2; \{\bar{\mathbf{I}}\}) = 0, \quad (77)$$

subtract the two equations and integrate by parts.

For $g + g \rightarrow \bar{b} + b + PX$ where X is an off-shell SM Higgs boson or an on-shell BSM Higgs boson the first three invariants in Eq.(70) are

$$s_{1-} \leq s_1 \leq s_{1+}, \dots, t_{0-} \leq t_0 \leq t_{0+}, \quad (78)$$

and we introduce new, scaled variables,

$$s_1 = (s_{1+} - s_{1-})y_1 + s_{1-}, \dots, t_0 = (t_{0+} - t_{0-})y_3 + t_{0-}. \quad (79)$$

For the last invariant in Eq.(70) we use $\lambda_1 = \lambda(s, s_1, m_b^2)$ and $\lambda_3 = \lambda(s, u_1, M^2)$ and define

$$\xi = (s - s_1 + 2t_0 - m_b^2) \lambda_1^{-1/2}, \quad \eta = \left[2s(s_1 + M^2) - (s + s_1)(s - u_1 + M^2) - m_b^2(s + u_1 - M^2)\right] (\lambda_1 \lambda_3)^{-1/2}. \quad (80)$$

Next we introduce

$$z = \pi \left(y_4 - \frac{1}{2}\right), \quad y_4 \in [0, 1], \quad (81)$$

and obtain

$$t_1 = \frac{1}{2} \left\{ [(\xi \eta)^{1/2} \sin(z) + \xi \eta] \lambda_3^{1/2} - s + u_1 + M^2 \right\}. \quad (82)$$

The object of interest (fully differential) is

$$\frac{d^4 \sigma}{dy_1 \dots dy_4} = \frac{1}{32 \pi^3} \frac{s_{1+} - s_{1-}}{512 s_1 s^2} (\lambda_1 \lambda_2)^{1/2} \sum_{s,c} |A|^2, \quad (83)$$

where $\lambda_1 = \lambda(s, s_1, m_b^2)$ and $\lambda_2 = \lambda(s_1, M^2, m_b^2)$. The sum is over spin and color, A is the amplitude. Finally,

$$s_{1-} = (M + m_b)^2, \quad s_{1+} = (\sqrt{s} - m_b)^2. \quad (84)$$

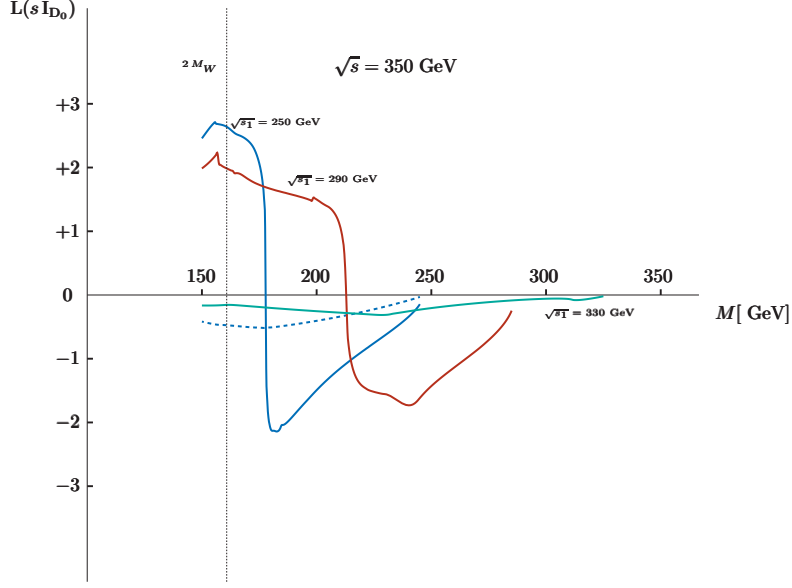


Figure 18: D_0 -function integrated over u_1 at $\sqrt{s} = 350 \text{ GeV}$ and for three values of s_1 .



Figure 19: Family b) for $g(Q) \rightarrow b(q_1) + \bar{b}(q_3) + H(q_2)$.

Both LO and interference with one-loop corrections are proportional to m_b^2 while one-loop squared survives the limit $m_b \rightarrow 0$. Loop effects are suppressed by a factor $g^2/(16\pi^2) = 0.0027$ which, however is of the same order of magnitude of the Yukawa suppression $m_b^2/M_W^2 \approx 0.0021$. Therefore, we expect one-loop squared to be of the same order of the interference.

We selected $\sqrt{s} = 865 \text{ GeV}$ and $M = 308.06 \text{ GeV}$. In the four-dimensional y -space there are trajectories feeling the presence of the Peierls zero, for instance, with $y_3 = y_4 = 0.3$ and $y_2 = 0.6$ we have (NNLO is up to one-loop squared)

	$y_1 = 0.25$	$y_1 = 0.2626$	$y_1 = 0.27$
$\delta_{\text{NLO}}^{\text{AT}} [\%]$	8.14	3.66	8.41
$\delta_{\text{NNLO}}^{\text{AT}} [\%]$	87.03	370.25	84.32

It is worth noting the very large NNLO effect, induced by the “ π^2 ” terms which originates from triangles, as explained in subsection 5.1.2. For comparison we give $\delta_{\text{NNLO}}^{\text{AT}}$ for different values of \sqrt{s} with M fixed and $y_1 = 0.2626$, $y_2 = 0.6$, $y_3 = y_4 = 0.3$:

$\sqrt{s} [\text{GeV}]$	350	550	865
$\delta_{\text{NNLO}}^{\text{AT}}$	-0.68	10.56	370.25

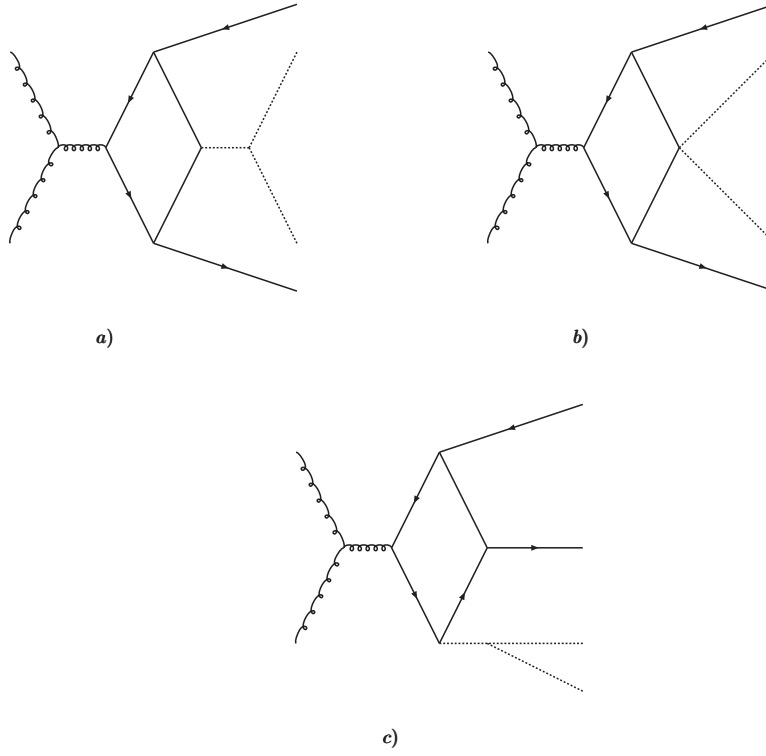


Figure 20: Diagrams contributing to $g + g \rightarrow \bar{b} + b + H + H$.

showing the combined effect of the Peierls zero and the “ π^2 ” terms. Unfortunately, when more (y) integrations are performed the effect becomes less and less visible; for instance in the two-dimensional distribution, $y_1 - y_2$, trajectories are almost flat in the $y_1(y_2)$ direction. This seems to be a general result: for processes requiring more and more invariants the fully inclusive observables become less and less sensitive to ATs.

5.3. The process $g + g \rightarrow \bar{b} + b + H + H$

There are several classes of diagrams contributing to the process. In Figure 20 diagrams of class a) have an AT inside the physical region; diagrams of class b) do not have an AT but are needed for gauge invariance when we move beyond the D_0 -approximation. Diagrams in Figure 21 include pentagons which do not have a leading singularity in the physical region but show a subleading one (box driven) obtained by shrinking one line of the pentagon to a point.

6. Pentagons

As shown in Ref. [52] there is no discontinuity associated with the LLS of the pentagon. This is why Ref. [65] refers to the singularity as a pole, i.e. $E_0 \sim 1/\Delta_5$, as shown in Ref. [51].

Consider the diagram of Figure 22 with $Q^2 = -s$, $q_i^2 = -M_i^2$. The corresponding process is described in terms of the following set of invariant:

$$s_1 = -(Q - q_1)^2, \quad s_2 = -(Q - q_1 - q_2)^2, \quad u_1 = -(Q - q_2)^2, \quad u_2 = -(Q - q_3)^2, \quad t_2 = -(Q - q_2 - q_3)^2. \quad (85)$$

Their limits, the physical region, are:

$$(M_2 + M_3 + M_4)^2 \leq s_1 \leq (\sqrt{s} - M_1)^2, \quad (M_3 + M_4)^2 \leq s_2 \leq (\sqrt{s_1} - M_2)^2, \quad (86)$$

and $u_{1-} \leq u_1 \leq u_{1+}$ etc. where the limits can be written as $u_{1\pm} = u_{10} \pm du_1$ etc. with the following explicit expressions (see Ref. [91] for details),

$$u_{10} = s + M_2^2 - \frac{1}{2s_1} (s_1 - s_2 + M_2^2)(s + s_1 - M_1^2), \quad \Delta u_1 = \frac{1}{2s_1} \lambda_1 \lambda_2,$$

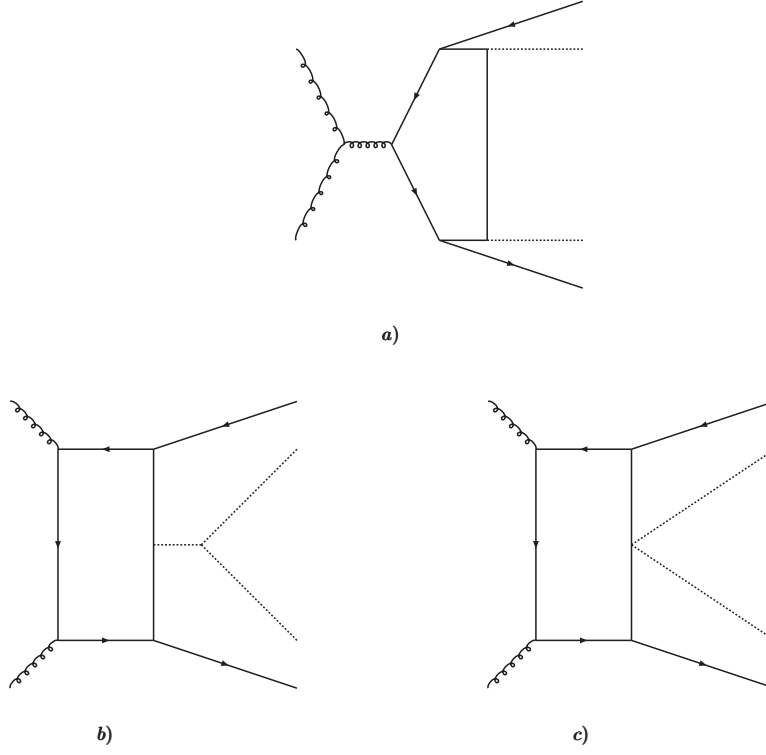


Figure 21: Diagrams contributing to $g + g \rightarrow \bar{b} + b + H + H$.

$$\begin{aligned}
 u_{20} &= s + M_3^2 - \frac{1}{2s_2} (s_2 + M_3^2 - M_4^2) (s + s_2 - s'_2), & \Delta u_2 &= \frac{1}{2s_2} \lambda_3 \lambda_4, \\
 t_{20} &= u_1 + M_3^2 - \frac{1}{2s} (s - u_2 + M_3^2) (s + u_1 - M_2^2) - \frac{1}{2} \frac{\xi_2 \eta_2}{s} \lambda_5 \lambda_6, & dt_2 &= \frac{1}{2s} (1 - \xi_2^2)^{1/2} (1 - \eta_2^2)^{1/2} \lambda_5 \lambda_6.
 \end{aligned} \quad (87)$$

Variables $\lambda_1, \dots, \lambda_6$ are defined in terms of the following Källén lambda functions:

$$\begin{aligned}
 \lambda_1 &= \lambda^{1/2}(s, s_1, M_1^2), & \lambda_2 &= \lambda^{1/2}(s_1, s_2, M_2^2), & \lambda_3 &= \lambda^{1/2}(s, s_2, s'_2), \\
 \lambda_4 &= \lambda^{1/2}(s_2, M_3^2, M_4^2), & \lambda_5 &= \lambda^{1/2}(s, u_1, M_2^2), & \lambda_6 &= \lambda^{1/2}(s, u_2, M_3^2).
 \end{aligned} \quad (88)$$

We have also introduced additional variables

$$s'_2 = s - s_1 + s_2 - u_1 + M_1^2 + M_2^2, \quad t'_1 = M_2^2. \quad (89)$$

The variables ξ_2 and η_2 can be found in Ref. [91] with full details on the calculation of the phase space.

The example to be discussed is as follows:

$$\begin{aligned}
 M_1 &= m_b, & M_3 &= 0, & M_2 &= M, & M_4 &= m_b, \\
 m_1 &= m_t, & m_2 &= M_W, & m_3 &= 0, & m_4 &= M_W, & m_t &= m_t,
 \end{aligned} \quad (90)$$

where q_3 is an electron and we have neglected the mass while line 3 is a neutrino. In the limit of zero widths the equation $\Delta_5 = 0$ is quadratic in t_2 ; here q_2 is the momentum of a pair, electron-photon, so that what we are considering is $gg \rightarrow g \rightarrow \bar{b} b e^- e^+ \gamma$. An example of physical-region ATs is given in the following table.

fixed					solution	
M_2 [GeV]	$\sqrt{s_1}$ [GeV]	$\sqrt{s_2}$ [GeV]	$\sqrt{u_1}$ [GeV]	$\sqrt{u_2}$ [GeV]	$\sqrt{t_2}$ [GeV]	
97.40	260.47	139.17	201.03	275.84	122.53	
"	"	"	203.55	260.91	89.06	
"	"	"	"	265.74	103.56	
"	"	"	"	270.56	117.37	
"	"	"	"	275.39	130.91	
"	"	147.14	213.31	266.39	121.68	
"	"	"	"	271.07	138.30	
"	"	"	215.30	255.98	98.96	
"	"	"	"	260.89	113.19	

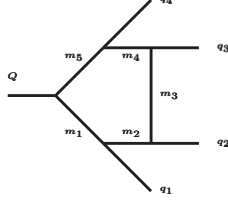


Figure 22: Pentagon diagram: the general case with arbitrary internal and external masses.

The same line of arguments applies to $gg \rightarrow \bar{b}b\bar{u}u$ or $gg \rightarrow \bar{b}b\bar{d}d$, with $u \neq t$.

An interesting question is the following: consider a particle of invariant mass \sqrt{s} “decaying” into a four-body final state; Δ_5 is a quartic polynomial in s and we look for complex solutions in the variable s to the equation $\Delta_5 = 0$ with $0 < \text{Re}X_4 < \dots < \text{Re}X_1 < 1$. Since the AT for a pentagon is a pole this is exactly the situation where the AT could be misinterpreted as the peak due to an unstable particle.

Deciding whether it is a resonance would require establishing that the “pole” is on the second (unphysical) sheet. In this case one of the external ‘masses’, i.e. s , is complex and $\ln^-(z) \neq \ln(z)$ etc. This fact requires a more complicated structure of the analytic continuation of the original integral including contour deformation, see section 6.6 of Ref. [82], which is beyond the scope of this work. Furthermore, the real analytic approach has the merit of working with quantities having a direct physical meaning and direct physical intuition is certainly of great help. The vertex function with three complex external masses has been discussed in Ref. [94].

7. Hexagons

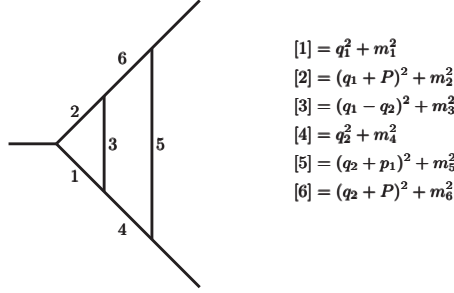
For six point functions the leading Landau singularity is a sum of products of the Landau singularities for the reduced pentagon diagrams [52].

For $n \geq 6$ all the singularities of the one-loop n -point functions coincide with the singularities of the reduced, down to and including the pentagon, diagrams obtained from the main diagram [95, 96]. This result follows from the well-known property of vanishing of Gram determinants if any of its principal minors vanish. A plausible conclusion: at one loop a simple pole is the strongest possible singularity.

8. Two loop diagrams

So far we have discussed the leading Landau singularity for one-loop diagrams. In view of the impact of QCD corrections we would like to understand the behavior of two loop diagrams; this is, by far, more complicated than the one loop analysis, especially because we have no simple expression for the BST factor. Therefore, we have to resort to the set of Landau equations, written in momentum space. The full analysis for two loop triangles has been given in Ref. [97] and we will use the relevant results. For a diagram with l loops and n propagators we have $4l + n + 1$ conditions on $4l + n$ variables; this means that a solution may exist only for specific values of external momenta. Consider the vertex of Figure 23, the Landau equation for this topology are as follows:

$$\begin{aligned} \alpha_1 (q_1^2 + m_1^2) &= 0, & \alpha_2 ((q_1 + P)^2 + m_2^2) &= 0, & \alpha_3 ((q_1 - q_2)^2 + m_3^2) &= 0, \\ \alpha_4 (q_2^2 + m_4^2) &= 0, & \alpha_5 ((q_2 + p_1)^2 + m_5^2) &= 0, & \alpha_6 ((q_2 + P)^2 + m_6^2) &= 0, \end{aligned}$$



$$\begin{aligned}
[1] &= q_1^2 + m_1^2 \\
[2] &= (q_1 + P)^2 + m_2^2 \\
[3] &= (q_1 - q_2)^2 + m_3^2 \\
[4] &= q_2^2 + m_4^2 \\
[5] &= (q_2 + p_1)^2 + m_5^2 \\
[6] &= (q_2 + P)^2 + m_6^2
\end{aligned}$$

Figure 23: Two loop diagram. With $[i]$ we denote the inverse propagator for line i .

and also

$$\begin{aligned}
\alpha_1 q_{1\mu} + \alpha_2 (q_1 + P)_\mu + \alpha_3 (q_1 - q_2)_\mu &= 0, \\
-\alpha_3 (q_1 - q_2)_\mu + \alpha_4 q_{2\mu} + \alpha_5 (q_2 + p_1)_\mu + \alpha_6 (q_2 + P)_\mu &= 0,
\end{aligned} \tag{91}$$

The leading Landau singularity occurs for $\alpha_i \neq 0, \forall i$. We multiply the two equations Eq.(91) by $q_{1\mu}, q_{2\mu}, p_{1\mu}$ and P_μ , respectively. This gives an homogeneous system of eight equations. If all α_i are different from zero we may use

$$\begin{aligned}
q_1^2 &= -m_1^2, & q_2^2 &= -m_4^2, & q_1 \cdot q_2 &= \frac{1}{2} (m_3^2 - m_1^2 - m_4^2), \\
q_1 \cdot P &= -\frac{1}{2} (P^2 - m_1^2 + m_2^2), & q_2 \cdot p_1 &= -\frac{1}{2} (p_1^2 - m_4^2 + m_5^2), & q_2 \cdot P &= -\frac{1}{2} (P^2 - m_4^2 + m_6^2).
\end{aligned}$$

Compatibility requires a set of relations among $P^2, p_{1,2}^2$ and internal masses. If we select $m_3 = 0$ (gluon, photon), $m_5 = m_b$ and the remaining masses equal to m_t then a non trivial solution ($\alpha_i \neq 0, \forall i$) occurs iff

$$s = -P^2 = 4m_t^2, \quad M_1^2 = -p_1^2 = (m_t \pm m_b)^2, \quad M_2^2 = -p_2^2 = (m_t \mp m_b)^2, \tag{92}$$

i.e. exactly at the boundary of phase space. The solution is $\alpha_{1,3,4,5}$ arbitrary and $\alpha_2 = \alpha_1, m_t \alpha_6 = m_t \alpha_4 - m_b \alpha_5$. This solution includes the case $\alpha_3 = 0$.

It is worth noting that for physical configuration, i.e. the real external momenta, the Landau singularities are on the first (physical) sheet when $\alpha_i \in [0, 1]$ and may or may not be on the first (physical) sheet when $\alpha_i \notin [0, 1]$.

If $m_3 = M_Z$ we obtain $s = 4m_t^2 - M_Z^2$ and

$$\begin{aligned}
&2m_t^2 (M_1^2 + M_2^2)^2 - \left[8(m_t^2 + m_b^2)m_t^2 - (3m_t^2 + m_b^2) \right] (M_1^2 + M_2^2) - M_Z^2 m_t M_1^2 M_2^2 \\
&- \left[(m_t^2 + m_b^2)^2 + 4m_t^2 (m_t^2 + 2m_b^2) M_Z^2 + (m_t^2 + m_b^2) M_Z^4 + 8(m_t^2 + m_b^2)^2 m_t^2 \right] = 0.
\end{aligned} \tag{93}$$

It is easily seen that the last equation does not have real solutions for $M_{1,2}$ for physical values of M_Z, m_t and m_b .

9. Special cases

As we have seen any one-loop diagram with N external legs is characterized by its BST factor Δ_N defined in Eq.(8), $N - 1$ coefficients, X_1, \dots, X_{N-1} defined in Eq.(7) and by a set of external masses and Mandelstam invariants. In the

complex mass scheme we have $\Delta_N, X_i \in \mathbb{C}$. With no loss of generality, we fix $N = 4$ and consider a general process $Q \rightarrow q_1 + q_2 + q_3$ where $Q^2 = -s$ and $q_i^2 = -M_i^2$. Let s_1 and u_1 be the two independent invariants, defined in Eq.(54). Consider the following system of equations:

$$\begin{aligned} \operatorname{Re} \Delta_4 &= 0 & \operatorname{Im} \Delta_4 &= 0 \\ \operatorname{Im} X_i &= 0 & i &= 1, \dots, 3 \end{aligned}$$

Therefore we have 5 equations in 6 unknowns, $s, s_1, u_1, M_{1,2,3}^2$; a solution will give a surface parametrized by $s_1 = s_1(s), u_1 = u_1(s)$ etc. If the real part of the X_i , evaluated at the solution, is ordered then we may have a pinch singularity even in the complex mass scheme. The square of the box will be non-integrable.

For the pentagon we have 5 external masses and 5 invariants with 4 X variables, therefore 6 equations for 10 unknowns which, once again, gives a surface of potential singularities. If the $\operatorname{Re} X_i$ are ordered the pentagon itself may develop a non-integrable singularity, even in the complex mass scheme.

Having or not a singularity depends on which trajectory we follow in phase space, i.e. on the order of the two limits, $\Delta_N \rightarrow 0$ and $\operatorname{Im} X_i \rightarrow 0$.

The fate of these configurations can only be decided on a case-by-case basis; if they appear inside the physical region their study must be completed including beam energy spread, parton distribution functions and modelling lossy processes (e.g. by including a Crystal Ball function). An illustrative example is given in subsection 9.1.

We briefly mention one example, a box corresponding to $Q \rightarrow q_1 + q_2 + q_3$ where $Q^2 = -s$ and $q_i^2 = -M_i^2$. There are four internal lines with masses m_i ; when $m_1 = m_4$ and $m_2 = m_3$ we derive the following result: given $s_1 = -(q_2 + q_3)^2$ and $u_1 = -(q_1 + q_3)^2$, when

$$M_2 = \sqrt{s} - \sqrt{u_1}, \quad M_3^2 = \frac{s_1(u_1 - s) + M_2^2(s + s_1 + u_1 - 2M_1^2) - M_2^4}{s + M_2^2 - u_1}, \quad (94)$$

it follows that $\forall i, \operatorname{Im} X_i = 0$ and $\operatorname{Im} C_4 = 0$. However, on the hypersurface defined by Eq.(94) we have $G_4 = 0$. Therefore, the box is a linear combination of four triangles divided by C_4 .

We can now solve for $\operatorname{Re} C_4 = 0$ where $\operatorname{Re} C_4$ is a real polynomial of fourth degree in M_1^2 ; the solutions, $M_1^2(s_1, u_1)$, are the surfaces where $C_4 \rightarrow 0$ after $G_4 \rightarrow 0$ (this case is discussed in Appendix B). We are looking for solutions where $M_{1,2,3}^2 \in \mathbb{R}_{>0}$ and where s_1 and u_1 are within their boundaries for fixed s . These conditions are very difficult to satisfy and only in few cases we have found real positive (squared) masses and $M_2 + M_3 \leq \sqrt{s_1} \leq \sqrt{s} - M_1$. As far as u_1 is concerned we have found (with a scan in $s - s_1 - u_1$) that u_1 is always larger than its (physical) upper bound, even if in a very limited number of cases the difference $\sqrt{u_1} - \sqrt{u_{1+}}$ can be as small as 1 eV .

9.1. Folding the AT

Consider a process $e^+e^- \rightarrow X$; in the so-called ‘‘radiator approach’’ the hard scattering cross section is convoluted with initial state QED radiation,

$$\sigma(s) = \int_0^1 dz H(z, s) \hat{\sigma}((1-z)s), \quad (95)$$

where $s = 4E^2$, E being the beam energy. We are not concerned here with the exact form of the radiator, it will be enough to assume the so-called virtual-soft approximation where

$$H = H_0 \beta z^{\beta-1}, \quad 0 < \beta \ll 1. \quad (96)$$

The simple example we have in mind is

$$F(s) = \int_0^1 dz H(z, s) f(s), \quad f(s) = \int_0^1 dx \chi^{-3/2}(x, s), \quad (97)$$

where $\chi = sx + (m_2^2 - m_1^2 - s)x + m_1^2$. We introduce

$$s_p = (m_1 - m_2)^2, \quad s_t = (m_1 + m_2)^2, \quad \lambda = (s - s_p)(s - s_t), \quad (98)$$

and consider the behavior of $f(s)$ around the normal threshold s_t . We obtain

$$f(s) = -8 \frac{s^{1/2}}{\lambda} + \text{reg. terms} \quad s \rightarrow s_t. \quad (99)$$

The function has a simple pole at the normal threshold. Inserting this result into Eq.(97) we obtain

$$\begin{aligned} F(s) &= 8H_0 \beta \frac{s^{1/2}}{s_t - s_p} (s - s_t)^{-1} J(s) + F_p(s), \\ J(s) &= \int_0^1 dx x^{\beta-1} (1-x)^{1/2} \left(1 + \frac{s}{s_t - s} x\right)^{-1}. \end{aligned} \quad (100)$$

The integral in J gives

$$J(s) = B\left(\frac{3}{2}, \beta\right) K(s), \quad K(s) = {}_2F_1\left(1, \beta; \beta + \frac{3}{2}; \frac{s}{s - s_t}\right), \quad (101)$$

where ${}_2F_1$ is the hypergeometric function and B is the Euler beta function. For $s \rightarrow s_t$ we use well-known properties of the hypergeometric function and obtain

$$K(s) = B_1 \rho^{-1} {}_2F_1\left(1, \frac{1}{2} - \beta; 2 - \beta; \rho^{-1}\right) + B_2 \rho^{-\beta} {}_2F_1\left(-\frac{1}{2}, \beta; \beta; \rho^{-1}\right), \quad (102)$$

where we have introduced

$$\rho = \frac{s}{s_t - s}, \quad B_1 = \frac{\beta + 1/2}{\beta - 1}, \quad B_2 = 2\pi^{-1/2} \Gamma(\beta + 3/2) \Gamma(1 - \beta). \quad (103)$$

Therefore, the leading behavior of K is given by

$$K(s) \sim B_2 s^{-\beta} \left(\frac{s_t}{s}\right)^{1/2} (s_t - s)^\beta, \quad s \rightarrow s_t. \quad (104)$$

In terms of the folding this means that $F(s) \sim (s_t - s)^{\beta-1}$ which is integrable and can be used in the convolution with the beam energy spread¹⁰. When masses become complex, $m_i^2 \rightarrow m_i^2 - im_i\Gamma_i$, the zeros of λ also become complex and the solutions of $\text{Re } \lambda = 0$ move above s_t and below s_p by a quantity proportional to the widths.

10. AT beyond the SM

As mentioned, a physical-region singularity requires a theory with a hierarchy of heavy masses: therefore, ATs hardly appear in the SM. However any BSM theory with an heavy neutral Higgs boson (H) and a charged one (H^\pm) satisfying $M_H > 2M_{H^\pm}$ and $M_{H^\pm} > M_W + M_Z$ will have an AT in the decay $H \rightarrow ll\nu\nu$. One could even imagine a situation with a light Higgs boson h and 3 heavy Higgs bosons, $H_{1,2,3}$, where $M_{H_1} > 2M_{H_2}$, $M_{H_2} > M_{H_3} + M_h$ and $M_{H_3} > 3M_h$ giving an AT in the pentagon corresponding to $H_1 \rightarrow 6h$.

There are also specific examples from a supersymmetric context, namely the production of a heavy neutral Higgs and a pair of massless b -quarks by gluon fusion, via a loop containing two squarks (sbottoms) and two neutralinos; for instance we mention AT effects in Higgs decays into charginos and neutralinos in the complex MSSM [98].

In general the large multiplicity of (super)fields introduced in non-minimal Susy-GUT models will result in the development of a Landau singularity. Another example is given by $M_{H^\pm} > m_t + m_b$ in the decay $H \rightarrow \bar{t} + t$. In general we can say that whenever the initial and final states have more than two particles, the scattering matrix gets a contribution from diagrams where there are singularities for physical values of the energies and momenta [7].

¹⁰The influence of radiation and energy spread was suggested, long ago, in a private discussion by Thomas Binoth.

11. Conclusions

Anomalous thresholds have been studied by physicists since the 1950's, e.g. electromagnetic scattering off a deuteron: A fast falloff of the form factor of loosely bound deuteron is due to the presence of the anomalous singularity close to the physical region of the scattering reaction; if not for the anomalous singularity, the scattering amplitude would have only vary at a much larger scale of the two-proton threshold.

Causality ensures that scattering amplitudes are analytic functions of momenta and an analytic function is characterized by its singularities. Furthermore, each scattering function has physical-region singularities only on positive- α Landau surfaces [85] and near these surfaces it is the limit from certain well-defined directions of a unique analytic function.

In this work the matrix element corresponding to the general one-loop Feynman diagram is rigorously investigated in detail. We have given a general classification of the one-loop - physical-region - leading Landau singularities (the so-called anomalous thresholds) for LHC processes, taking into account that the position of each singularity is determined by masses and invariants while the character of the singularity derives from the topology of the interaction process.

Our methodology is based on finding zeros of Cayley determinants with constraints. The advantage of the approach is that the condition for an AT is written directly in the space of invariants instead of being obtained through a set of consistency equations in $+\alpha$ Landau surfaces.

The main motivation was to find observable effects, e.g.. peaks in distributions; indeed, resonances are normally observed as peaks in certain invariant mass distributions. However, is a peak necessarily due to the presence of a resonance? Are there peaks produced by kinematic singularities? It is well known that scattering amplitudes also possess singularities corresponding to more complicated types of particle exchanges: these are indeed the Landau singularities. A well-know example is that there has been interest for many years in trying to use the triangle singularity to explain certain enhancements in strongly interacting three-particle final states.

We have found that peaks, when present, are marginal and the main result of our work is that the radiative corrections induced by physical-region ATs are well under control once regularized with the complex mass scheme; nevertheless they should be taken into account in estimating the missing higher order uncertainty [99]. When assessing such results, it should be borne in mind that Yukawa suppressed LO processes can be heavily influenced by NLO corrections, i.e. NLO is the first relevant term.

We need to acknowledge the fact that we do not have a fully satisfactory (gauge) theory of unstable particles, despite past [100, 101] and recent progress [5, 6]. However, the complex mass scheme is essential in this context, given the non-integrable character of the ATs for boxes and pentagons (if internal masses are kept real). From this point of view we are tempted to argue for a definition of a “natural” theory as the one where there are no ATs inside the physical region. To summarize - with anomalous thresholds non-integrable functions may enter into physical calculations, and the attempt to interpret these integrals and find useful solutions can lead us to a broader understanding of the physical situation.

The SM is almost “natural”: physical-region ATs are exceptional for SM, on-shell, LHC physics but more frequent in the so-called “off-shell” LHC physics and in BSM models; the reason for that is immediately seen in the context of the Coleman-Norton [28] and Kershaw [42] theorems, i.e. not enough heavy masses in the SM to be in one of the 6(14) branches of the physical-region Landau curve for a triangle (box) diagram.

We have discussed how the introduction of complex masses gives rise to new configurations, the Peierls zeros (defined in Eq.(19)). Furthermore, we have shown in section 9 that boxes and pentagons with arbitrary external masses may develop non-integrable singularities even when regularized by the complex mass scheme.

We have also discussed the folding of anomalous amplitudes, e.g. with QED radiation, in section 9.1.

A final result, discussed in section 4.1, is the following: for e^+e^- , $\bar{q}q$ and gg initial states there are amplitudes where the initial state couples to a neutral object which can couple to WW or $t\bar{t}$. In these cases we can have $b\bar{b}g$ and $f\bar{f}g$ final

states producing a singularity at large $f(\bar{f})-g(\gamma)$ invariant masses, on top of the more familiar infrared and collinear ones.

To conclude we can say that the most elementary form of Landau singularities is connected to holomorphic functions defined by integrals of rational functions as they appear in the “perturbative” approach to quantum field theory. From a mathematical point of view these holomorphic structures have a deeper meaning and general questions (are Landau singularities effectively singular “somewhere”?) should receive an answer in this context.

Appendix A. Technical details

Production and decay processes are described in terms of Mandelstam invariants where, for a $n \rightarrow m$ process, we have $3(n+m) - 10$ independent invariants.

Consider a process $N \rightarrow 0$ with all incoming momenta; a convenient way of describing the boundaries of the phase space, the relations between vectors and invariants and the non-linear constraints that arise when $N \geq 6$ is the following. If at least one momentum is such that $p_i^2 \neq 0$ we redefine n -dimensional momenta and introduce components

$$p_1^\mu \equiv (\vec{0}, m_1). \quad (\text{A.1})$$

Then we introduce

$$(h^N)_{ij} = p_i \cdot p_j, \quad i, j = 1, \dots, N, \quad h^{N;kl} = h^N \quad \text{with row } k \text{ and column } l \text{ removed.} \quad (\text{A.2})$$

The vector p_2 is defined by

$$p_2^\mu \equiv \left(\vec{0}, \sqrt{\frac{\det h^2}{\det h^1}}, -\frac{h_{12}^2}{m_1} \right). \quad (\text{A.3})$$

Next n -dimensional vectors will be

$$\begin{aligned} p_3^\mu &\equiv \left(\vec{0}, -\frac{\det h^{3;32}}{\sqrt{\det h^1 \det h^2}}, \sqrt{\frac{\det h^3}{\det h^2}}, -\frac{h_{13}^3}{m_1} \right), \\ p_4^\mu &\equiv \left(\vec{0}, -\frac{\det h^{4;43;32}}{\sqrt{\det h^1 \det h^2}}, \frac{\det h^{4;43}}{\sqrt{\det h^2 \det h^3}}, \sqrt{\frac{\det h^4}{\det h^3}}, -\frac{h_{14}^4}{m_1} \right), \end{aligned} \quad (\text{A.4})$$

etc. If $N = 5$ then momentum conservation gives $p_5 = -\sum p_i$. If, instead $N = 6$, p_6 follows from momentum conservation whereas p_5 requires a fifth component; if $d = 4$ the vanishing of the fifth component requires $\det h^5 = 0$.

Our convention for selecting independent invariants and their boundaries follows Ref. [91]. Loop integrals follow from Ref. [51], i.e. we perform numerical integration over Feynman parameters and Mandelstam invariants in one stroke. It is worth noting that instabilities due to zeros of Gram determinants are absent in this approach. The typical integrals to be evaluated are of the following form:

$$\mathcal{O}_\alpha = \int d\{I\} \int dS_N \sum_{j_1=0}^{J_1} \dots \sum_{j_N=0}^{J_N} F_{j_1 \dots j_N}(\{I\}) x_1^{j_1} \dots x_N^{j_N} \left[(x - X_{N+1})^t H (x - X_{N+1}) + \Delta_{N+1} \right]^{-\alpha}, \quad (\text{A.5})$$

where $\{I\}$ denotes the set of Mandelstam invariants.

Kershaw theorem proves factorization of the scattering amplitude in the vicinity of the given Landau singularity but also that, for a given set of invariants which lie on the given physical-region Landau singularity, the loop momentum is uniquely determined. This means that, in the vicinity of the singularity, all loop integrals are scalar. In Feynman parameter space this can be seen as follows:

$$\mathcal{O}_\alpha \Big|_{\text{AT}} \sim \int d\{I\} \sum_{j_1=0}^{J_1} \dots \sum_{j_N=0}^{J_N} F_{j_1 \dots j_N}(\{I\}) X_1^{j_1} \dots X_N^{j_N} \int dS_N \left[(x - X_{N+1})^t H (x - X_{N+1}) + \Delta_{N+1} \right]^{-\alpha}. \quad (\text{A.6})$$

Appendix A.1. The phase-space integral for $gg \rightarrow \bar{b}bX$

Consider the process

$$g(p_1) + g(p_2) \rightarrow b(q_1) + X(q_2) + \bar{b}(q_3), \quad (\text{A.7})$$

with $s = -(p_1 + p_2)^2$, $p_i^2 = 0$, $q_{1,3}^2 = -m_b^2$ and $q_2^2 = M^2$. We introduce

$$\lambda_1 = \lambda(s, s_1, m_b^2), \quad \lambda_2 = \lambda(s_1, M^2, m_b^2), \quad \lambda_3 = \lambda(s, u_1, M^2) \quad (\text{A.8})$$

and auxiliary quantities

$$\begin{aligned} \xi &= \lambda_1^{-1/2} (s - s_1 + 2t_0 - m_b^2), \\ \eta &= (\lambda_1 \lambda_3)^{-1/2} \left[2s(s_1 + M^2 - m_b^2) - (s - u_1 + M^2)(s + s_1 - m_b^2) \right], \\ \omega &= \lambda_3^{-1/2} (s - u_1 + 2t_0 - M^2), \\ \zeta &= (1 - \eta^2)^{-1/2} (1 - \xi^2)^{-1/2} (\omega - \xi \eta). \end{aligned} \quad (\text{A.9})$$

The corresponding phase-space integral is

$$\int d\Phi = \frac{\pi}{2} \int_{s_{1-}}^{s_{1+}} ds_1 \int_{u_{1-}}^{u_{1+}} du_1 \int_{t_{0-}}^{t_{0+}} dt_0 \int_{t_{1-}}^{t_{1+}} dt_1 (\lambda_1 \lambda_3)^{-1/2} \left[(1 - \eta^2)(1 - \xi^2)(1 - \zeta^2) \right]^{-1/2}. \quad (\text{A.10})$$

The boundaries are

$$s_{1-} = (M + m_b)^2, \quad s_{1+} = (\sqrt{s} - m_b)^2, \quad u_{1\pm} = u_{10} \pm \Delta u_1, \quad \text{etc.} \quad (\text{A.11})$$

$$\begin{aligned} u_{10} &= s + M^2 - \frac{1}{2s_1} (s_1 + M^2 - m_b^2)(s + s_1 - m_b^2), \\ t_{00} &= m_b^2 - \frac{1}{2} (s - s_1 + m_b^2), \\ t_{10} &= M^2 - \frac{1}{2} (s - u_1 + M^2) + \frac{1}{2} \lambda^{1/2} \xi \eta, \end{aligned} \quad (\text{A.12})$$

$$\Delta u_1 = \frac{1}{2} \frac{(\lambda_1 \lambda_2)^{1/2}}{s_1}, \quad \Delta t_0 = \frac{1}{2} \lambda_1^{1/2}, \quad \Delta t_1 = \frac{1}{2} \lambda_3^{1/2} \left[(1 - \eta^2)(1 - \xi^2) \right]^{1/2}. \quad (\text{A.13})$$

Introducing dimensionless variables,

$$s_1 = (s_{1+} - s_{1-})y_1 + s_{1-}, \quad u_1 = 2\Delta u_1 y_2 + u_{1-}, \quad \text{etc.}, \quad (\text{A.14})$$

we obtain

$$\int d\Phi = \frac{\pi}{2} (s_{1+} - s_{1-}) \int \prod_{i=1}^4 dy_i \frac{(\lambda_1 \lambda_2)^{1/2}}{s_1 (1 - \zeta^2)^{1/2}}. \quad (\text{A.15})$$

Alternatively, we observe that $\zeta(t_{1\pm}) = \pm 1$ and

$$\int_{t_{1-}}^{t_{1+}} dt_1 = \frac{1}{2} \int_{-1}^{+1} d\zeta \left[\lambda_3 (1 - \xi^2)(1 - \eta^2) \right]^{1/2}, \quad (\text{A.16})$$

introduce

$$\zeta = \sin z, \quad z = \pi y_4 - \frac{1}{2} \pi, \quad (\text{A.17})$$

and derive

$$\int d\Phi = \frac{\pi^2}{4} (s_{1+} - s_{1-}) \int \prod_{i=1}^4 dy_i \frac{(\lambda_1 \lambda_2)^{1/2}}{s_1}. \quad (\text{A.18})$$

In this way the phase-space integral is mapped into the unit, four-dimensional, cube.

Appendix A.2. Momenta and invariants: an example

Consider the process

$$\mathbf{g}(p_1) + \mathbf{g}(p_2) \rightarrow \mathbf{b}(q_1) + \mathbf{H}(q_2) + \mathbf{H}(q_3) + \bar{\mathbf{b}}(q_4), \quad (\text{A.19})$$

momentum conservation gives $q_4 = P - q_1 - q_2 - q_3$ where $P = p_1 + p_2$. There are 8 invariants¹¹ defined by [91]:

$$\begin{aligned} s &= -(p_1 + p_2)^2, \\ s_i &= -\left(P - \sum_{j=1}^i q_j\right)^2, \quad i = 1, 2, \\ u_i &= -(P - q_{i+1})^2, \quad i = 1, 2, \\ t_i &= -(p_1 - q_{i+1})^2, \quad i = 0, 1, 2. \end{aligned} \quad (\text{A.20})$$

The linear relations among scalar products, $T_{ij} = p_i \cdot q_j$, $S_{ij} = q_i \cdot q_j$ and invariants are as follows:

$T_{11} = \frac{1}{2}(t_0 - m_b^2)$	$T_{12} = \frac{1}{2}(t_1 - M_H^2)$	$T_{13} = \frac{1}{2}(t_2 - M_H^2)$	$T_{14} = \frac{1}{2}(m_b^2 - t_0 - t_1 - t_2 - s) + M_H^2$
$T_{21} = \frac{1}{2}(s_1 - t_0 - s)$	$T_{22} = \frac{1}{2}(u_1 - t_1 - s)$	$T_{23} = \frac{1}{2}(u_2 - t_2 - s)$	$T_{24} = \frac{1}{2}(t_0 + t_1 + t_2 - u_1 - u_2 - s_1) + s$
$S_{12} = \frac{1}{2}(s_1 - s_2 + u_1 - s)$	$S_{13} = \frac{1}{2}(s_2 + u_2 - s - m_b^2) - S_{23}$	$S_{14} = \frac{1}{2}(s - u_1 - u_2) + m_b^2 + S_{23}$	
$S_{24} = \frac{1}{2}(s_2 - s_1 + M_H^2) - S_{23}$	$S_{34} = \frac{1}{2}(M_H^2 + m_b^2 - s_2)$		

Table A2: The linear relations among scalar products for process Eq.(A.19).

One scalar product remains free. To fix it we proceed as follows:

1. Go to the c.m.s with p_1 and p_2 along the z-axis and $p_1 \cdot p_2 = -s/2$.
2. Put q_1 in the x - z plane and fix its components (with $q_1^2 = -m_b^2$) in terms of $p_1 \cdot q_1$ and $p_2 \cdot q_2$.
3. Add the y-component for q_2 and fix q_2 (with $q_2^2 = -M_H^2$) in terms of the scalar products between q_2 and p_1, p_2, q_1 .
4. Introduce a fifth component for q_3 , derive q_3 (with $q_3^2 = -M_H^2$) in terms of the scalar products between q_3 and p_1, p_2, q_1, q_2 .
5. Replace scalar products in terms of invariants. The equation requiring this fifth component to be zero is a non-linear constraint, i.e. a quadratic equation in S_{23} with coefficients depending on the eight linearly independent invariants s, s_1, \dots, t_2 .

If we consider the subprocess

$$\mathbf{g} + \mathbf{g} \rightarrow \mathbf{b} + \bar{\mathbf{b}} + \mathbf{H}(\rightarrow \mathbf{H}\mathbf{H}), \quad (\text{A.21})$$

there is no need to introduce the full $2 \rightarrow 4$ kinematics and the phase space is a simple convolution of $2 \rightarrow 3$ and $1 \rightarrow 2$.

¹¹For $n \rightarrow m$ there are $3(n+m) - 10$ invariants.

Appendix B. One-loop integrals around their AT

In this appendix we present explicit results for the leading behavior of one-loop integrals around their physical-region AT; the original derivation was given in Ref. [51].

To extract the leading behavior of a triangle around its leading Landau singularity we introduce

$$C_{\square}(p_1, p_2; m_1, m_2, m_3) = C_0(p_1, p_2; m_1, m_2, m_3) + C_0(p_2, p_1; m_3, m_2, m_1). \quad (\text{B.1})$$

If the first C_0 in the r.h.s. of Eq.(B.1) is singular then the second is regular and

$$C_0(p_1, p_2; m_1, m_2, m_3) \sim C_{\square}(p_1, p_2; m_1, m_2, m_3). \quad (\text{B.2})$$

Given the quadratic forms

$$V_3(x_1, x_2) = x^t H x + 2K^t x + L, \quad (\text{B.3})$$

$$V^{(1)}(x) = V_3(0, x), \quad V^{(2)}(x) = V_3(x, 0), \quad \bar{V}^{(1)}(x) = V_3(1, x), \quad \bar{V}^{(2)}(x) = V_3(x, 1), \quad (\text{B.4})$$

consider two-dimensional bubbles

$$B_2^{(i)} = \int_0^1 dx \frac{1}{V^{(i)}(x)}, \quad \bar{B}_2^{(i)} = \int_0^1 dx \frac{1}{\bar{V}^{(i)}(x)}. \quad (\text{B.5})$$

We find

$$C_{\square} \sim -\frac{1}{2} \ln \Delta_3 \sum_{i=1,2} \left[X_i B_2^{(i)} + (1 - X_i) \bar{B}_2^{(i)} \right], \quad (\text{B.6})$$

for $\Delta_3 \rightarrow 0$. For generalized triangles we obtain

$$C_{\square}(i, j) \sim X_1^i X_2^j C_{\square}, \quad (\text{B.7})$$

as expected by the fact that the AT is a pinch singularity (and by the Kershaw theorem).

To extract the leading behavior of a box around its leading Landau singularity we introduce

$$D_{\square} = \sum_{\{123\}} \int dS_3 V_4^{-2}(x_1, x_2, x_3), \quad (\text{B.8})$$

where the sum is over the permutations of x_1, x_2, x_3 . The first term in the sum is the original D_0 function while the rest gives the five complementary functions which, by construction, are regular at the AT. As a consequence, we now have to evaluate D_0^{\square} when $\Delta_4 \approx 0$ and the point of coordinates X_i is inside the unit cube. We introduce

$$V^{(1)}(x_1, x_2) = V_4(0, x_1, x_2), \quad V^{(2)}(x_1, x_2) = V_4(x_1, 0, x_2), \quad V^{(3)}(x_1, x_2) = V_4(x_1, x_2, 0), \quad (\text{B.9})$$

$$\bar{V}^{(1)}(x_1, x_2) = V_4(1, x_1, x_2), \quad \bar{V}^{(2)}(x_1, x_2) = V_4(x_1, 1, x_2), \quad \bar{V}^{(3)}(x_1, x_2) = V_4(x_1, x_2, 1), \quad (\text{B.10})$$

where we have put $\Delta_4 = 0$, and consider the 3-dimensional \square -triangles

$$C_3^{(i)} = \int_0^1 dx_1 \int_0^{x_1} dx_2 \left[V^{(i)}(x_1, x_2) \right]^{-3/2}, \quad \bar{C}_3^{(i)} = \int_0^1 dx_1 \int_0^{x_1} dx_2 \left[\bar{V}^{(i)}(x_1, x_2) \right]^{-3/2} .. \quad (\text{B.11})$$

The result is

$$D_{\square} \sim \Gamma\left(\frac{1}{2}\right) \Delta_4^{-1/2} \sum_{i=1,3} \left[X_i C_3^{(i)} + (1 - X_i) \bar{C}_3^{(i)} \right]. \quad (\text{B.12})$$

The results of Eqs.(B.6)–(B.12) have been derived under the assumption that the corresponding Gram determinant is not vanishing. If this is not the case we will write the box(triangle) as a linear combination of four(three) triangles(bubbles) divided by the corresponding Cayley determinant [51]. An example will help in understanding; consider the following integral:

$$I = \int_0^1 dx \int_0^x dy \left[x^2 - \lambda y^2 + 2(ax - \lambda by) + L \right]^{-1}. \quad (\text{B.13})$$

In this case we derive

$$H = \begin{pmatrix} 1 & 0 \\ 0 & \lambda \end{pmatrix}$$

with $X_1 = -a, X_2 = b, G = \lambda$ and $C = L - a^2 - \lambda b^2$. We assume that $0 \leq b \leq -a \leq 1$ and derive the usual result

$$I \sim \ln \frac{C}{G}, \quad \Delta = \frac{C}{G} \rightarrow 0. \quad (\text{B.14})$$

However, if we take the limit $\lambda \rightarrow 0$ first then $G = 0$. In this case we obtain

$$I|_{\lambda=0} \sim (L - a^2)^{-1/2}, \quad L \rightarrow a^2, \quad (\text{B.15})$$

where $L - a^2$ is the Cayley determinant evaluated at $G = 0$. Therefore, the behavior is $C^{-1/2}$ and not $\ln \Delta$.

References

- [1] F.-K. Guo, Traps in hadron spectroscopy: Thresholds, triangle singularities, ..., PoS Hadron2017 (2018) 015. [arXiv:1712.10126](#). (1)
- [2] X.-H. Liu, U.-G. Meißner, Generating a resonance-like structure in the reaction $B_c \rightarrow B_s \pi \pi$, Eur. Phys. J. C77 (12) (2017) 816. [arXiv:1703.09043](#), [doi:10.1140/epjc/s10052-017-5402-8](#). (1)
- [3] X.-H. Liu, M. Oka, Q. Zhao, Searching for observable effects induced by anomalous triangle singularities, Phys. Lett. B753 (2016) 297–302. [arXiv:1507.01674](#), [doi:10.1016/j.physletb.2015.12.027](#). (1)
- [4] A. Denner, S. Dittmaier, The Complex-mass scheme for perturbative calculations with unstable particles, Nucl. Phys. Proc. Suppl. 160 (2006) 22–26, [22(2006)]. [arXiv:hep-ph/0605312](#), [doi:10.1016/j.nuclphysbps.2006.09.025](#). (1, 8)
- [5] S. Actis, G. Passarino, Two-Loop Renormalization in the Standard Model Part II: Renormalization Procedures and Computational Techniques, Nucl. Phys. B777 (2007) 35–99. [arXiv:hep-ph/0612123](#), [doi:10.1016/j.nuclphysb.2007.03.043](#). (1, 8, 32)
- [6] A. Denner, J.-N. Lang, The Complex-Mass Scheme and Unitarity in perturbative Quantum Field Theory, Eur. Phys. J. C75 (8) (2015) 377. [arXiv:1406.6280](#), [doi:10.1140/epjc/s10052-015-3579-2](#). (1, 8, 32)
- [7] R. E. Cutkosky, Anomalous thresholds, Rev. Mod. Phys. 33 (1961) 448–455. [doi:10.1103/RevModPhys.33.448](#).
URL <https://link.aps.org/doi/10.1103/RevModPhys.33.448> (1, 5, 31)
- [8] S. Bloch, D. Kreimer, Feynman amplitudes and Landau singularities for 1-loop graphs, Commun. Num. Theor. Phys. 4 (2010) 709–753. [arXiv:1007.0338](#), [doi:10.4310/CNTP.2010.v4.n4.a4](#). (1)
- [9] D. Kreimer, Cutkosky Rules from Outer Space, PoS LL2016 (2016) 035. [arXiv:1607.04861](#). (1)
- [10] T. Dennen, I. Prlina, M. Spradlin, S. Stanojevic, A. Volovich, Landau Singularities from the Amplituhedron, JHEP 06 (2017) 152. [arXiv:1612.02708](#), [doi:10.1007/JHEP06\(2017\)152](#). (1)
- [11] F. Boudjema, L. D. Ninh, $b\bar{b}H$ production at the LHC: Yukawa corrections and the leading Landau singularity, Phys. Rev. D78 (2008) 093005. [arXiv:0806.1498](#), [doi:10.1103/PhysRevD.78.093005](#). (2)
- [12] N. Le Duc, Leading electroweak corrections to the process $pp \rightarrow b\bar{b}H$ in the standard model at the LHC, Acta Phys. Polon. Supp. 1 (2008) 411–414. (2)
- [13] H. S. Do, P. H. Khien, F. Yuasa, One- and two-loop integrals with XLOOPS-GiNaC, PoS CPP2010 (2010) 016. (2)
- [14] A. Denner, S. Dittmaier, T. Hahn, Radiative corrections to $ZZ \rightarrow ZZ$ in the electroweak standard model, Phys. Rev. D56 (1997) 117–134. [arXiv:hep-ph/9612390](#), [doi:10.1103/PhysRevD.56.117](#). (2)
- [15] T. Binoth, G. Heinrich, N. Kauer, A Numerical evaluation of the scalar hexagon integral in the physical region, Nucl. Phys. B654 (2003) 277–300. [arXiv:hep-ph/0210023](#), [doi:10.1016/S0550-3213\(03\)00052-X](#). (2)
- [16] M. Rodgers, Automation of one-loop corrections for multi-particle processes, Ph.D. thesis, Durham U. (2012).
URL http://etheses.dur.ac.uk/4460/1/MRodgers_PhD_thesis.pdf (2)
- [17] G. Ponzano, T. Regge, E. R. Speer, M. J. Westwater, The monodromy rings of one loop feynman integrals, Commun. Math. Phys. 18 (1970) 1–64. [doi:10.1007/BF01649638](#). (2, 5)
- [18] L. D. Landau, On analytic properties of vertex parts in quantum field theory, Nucl. Phys. 13 (1959) 181–192. [doi:10.1016/0029-5582\(59\)90154-3](#). (2)
- [19] N. Nakanishi, Classical motion of particles and the physical-region singularity of the feynman integral, Prog. Theor. Phys. 39 (1968) 768–771. [doi:10.1143/PTP.39.768](#). (2)
- [20] N. Nakanishi, Ordinary and anomalous thresholds in perturbation theory, Progress of Theoretical Physics 22 (1) (1959) 128–144. [arXiv:/oup/backfile/content_public/journal/ptp/22/1/10.1143/ptp.22.128/2/22-1-128.pdf](#), [doi:10.1143/PTP.22.128](#).
URL <http://dx.doi.org/10.1143/PTP.22.128> (2)
- [21] J. C. Taylor, Analytic Properties of Perturbation Expansions, Phys. Rev. 117 (1960) 261–265. [doi:10.1103/PhysRev.117.261](#). (2)
- [22] J. C. Polkinghorne, G. R. Screaton, The analytic properties of perturbation theory — i, II Nuovo Cimento (1955-1965) 15 (2) (1960) 289–300. [doi:10.1007/BF02860252](#).
URL <https://doi.org/10.1007/BF02860252> (2)
- [23] M. J. W. Bloxham, D. I. Olive, J. C. Polkinghorne, S-matrix singularity structure in the physical region. 1. properties of multiple integrals, J. Math. Phys. 10 (1969) 494–502. [doi:10.1063/1.1664866](#). (2)
- [24] M. J. W. Bloxham, D. I. Olive, J. C. Polkinghorne, S-matrix singularity structure in the physical region. 2. unitarity integrals, J. Math. Phys. 10 (1969) 545–552. [doi:10.1063/1.1664875](#). (2)
- [25] M. J. W. Bloxham, D. I. Olive, J. C. Polkinghorne, S-matrix singularity structure in the physical region. 3. general discussion of simple landau singularities, J. Math. Phys. 10 (1969) 553–561. [doi:10.1063/1.1664876](#). (2)
- [26] M. S. of Japan, K. Itō, N. Sugakkai, Encyclopedic Dictionary of Mathematics, no. v. 1 in Encyclopedic Dictionary of Mathematics, MIT Press, 1993.
URL <https://books.google.it/books?id=WHj09K6xEm4C> (2)
- [27] I. Prlina, M. Spradlin, S. Stanojevic, All-loop singularities of scattering amplitudes in massless planar theories [arXiv:1805.11617](#). (2)
- [28] S. Coleman, R. E. Norton, Singularities in the physical region, Nuovo Cim. 38 (1965) 438–442. [doi:10.1007/BF02750472](#). (2, 32)
- [29] R. J. Eden, Analytic structure of collision amplitudes in perturbation theory, Phys. Rev. 119 (1960) 1763–1783. [doi:10.1103/PhysRev.119.1763](#).
URL <https://link.aps.org/doi/10.1103/PhysRev.119.1763> (3)
- [30] I. J. R. Aitchison, Logarithmic Singularities in Processes with Two Final-State Interactions, Phys. Rev. 133 (1964) B1257–B1266. [doi:10.1103/PhysRev.133.B1257](#). (3)
- [31] R. E. Norton, On the quantum field theories leading to the Corben equations. (3)
- [32] J. B. Bronzan, Overlapping Resonances in Dispersion Theory, Physical Review 134 (1964) 687–697. [doi:10.1103/PhysRev.134.B687](#). (3)
- [33] R. J. Eden, P. V. Landshoff, J. C. Polkinghorne, J. C. Taylor, Acnodes and cusps on Landau curves, J. Mathematical Phys. 2 (1961) 656–663. [doi:10.1063/1.1703752](#).

- URL <https://doi.org/10.1063/1.1703752> (3)
- [34] J. B. Bronzan, C. Kacser, Khuri-treiman representation and perturbation theory, *Phys. Rev.* 132 (1963) 2703–2711. doi:10.1103/PhysRev.132.2703.
URL <https://link.aps.org/doi/10.1103/PhysRev.132.2703> (3)
- [35] C. Schmid, Final-state interactions and the simulation of resonances, *Phys. Rev.* 154 (1967) 1363–1375. doi:10.1103/PhysRev.154.1363.
URL <https://link.aps.org/doi/10.1103/PhysRev.154.1363> (3)
- [36] R. F. Peierls, Possible Mechanism for the Pion-Nucleon Second Resonance, *Phys. Rev. Lett.* 6 (1961) 641–643. doi:10.1103/PhysRevLett.6.641. (3, 6)
- [37] C. Goebel, Comments on Higher Resonance Models, *Phys. Rev. Lett.* 13 (1964) 143–146. doi:10.1103/PhysRevLett.13.143. (3)
- [38] C. J. Goebel, S. F. Tuan, W. A. Simmons, Comments on rescattering effects and the Schmid theorem, *Phys. Rev. D* 27 (1983) 1069. doi:10.1103/PhysRevD.27.1069. (3)
- [39] A. V. Anisovich, V. V. Anisovich, Rescattering effects in three particle states and the Schmid theorem, *Phys. Lett.* B345 (1995) 321–324. doi:10.1016/0370-2693(94)01671-X. (3)
- [40] P. Collas, R. E. Norton, Observable effects of the leading Landau singularity of the box graph, *Phys. Rev.* 160 (1967) 1346–1358. doi:10.1103/PhysRev.160.1346.
URL <https://link.aps.org/doi/10.1103/PhysRev.160.1346> (3, 19)
- [41] B. N. Valuev, Observable Effects of Singularities of Triangular and Square Graphs, in: *International School of Elementary Particle Physics, Herceg-Novi, Herceg-Novi, Yugoslavia, September 15-28, 1969, 1977*, pp. 151–175. (3)
- [42] D. Kershaw, Algebraic factorization of scattering amplitudes at physical Landau singularities, *Phys. Rev. D* 5 (1972) 1976–1982. doi:10.1103/PhysRevD.5.1976. (3, 10, 32)
- [43] G. Ossola, C. G. Papadopoulos, R. Pittau, Reducing full one-loop amplitudes to scalar integrals at the integrand level, *Nucl. Phys.* B763 (2007) 147–169. arXiv:hep-ph/0609007, doi:10.1016/j.nuclphysb.2006.11.012. (3)
- [44] Z. Bern, L. J. Dixon, D. C. Dunbar, D. A. Kosower, One loop n point gauge theory amplitudes, unitarity and collinear limits, *Nucl. Phys.* B425 (1994) 217–260. arXiv:hep-ph/9403226, doi:10.1016/0550-3213(94)90179-1. (3)
- [45] C. F. Berger, Z. Bern, L. J. Dixon, D. Forde, D. A. Kosower, Bootstrapping One-Loop QCD Amplitudes with General Helicities, *Phys. Rev. D* 74 (2006) 036009. arXiv:hep-ph/0604195, doi:10.1103/PhysRevD.74.036009. (3)
- [46] Z. Bern, N. E. J. Bjerrum-Bohr, D. C. Dunbar, H. Ita, Recursive calculation of one-loop QCD integral coefficients, *JHEP* 11 (2005) 027. arXiv:hep-ph/0507019, doi:10.1088/1126-6708/2005/11/027. (3)
- [47] R. Britto, B. Feng, P. Mastrolia, The Cut-constructible part of QCD amplitudes, *Phys. Rev. D* 73 (2006) 105004. arXiv:hep-ph/0602178, doi:10.1103/PhysRevD.73.105004. (3)
- [48] R. K. Ellis, W. T. Giele, G. Zanderighi, The One-loop amplitude for six-gluon scattering, *JHEP* 05 (2006) 027. arXiv:hep-ph/0602185, doi:10.1088/1126-6708/2006/05/027. (3)
- [49] C. Anastasiou, R. Britto, B. Feng, Z. Kunszt, P. Mastrolia, D-dimensional unitarity cut method, *Phys. Lett.* B645 (2007) 213–216. arXiv:hep-ph/0609191, doi:10.1016/j.physletb.2006.12.022. (3)
- [50] F. Cachazo, Sharpening The Leading Singularity arXiv:0803.1988. (3)
- [51] A. Ferroglia, M. Passera, G. Passarino, S. Uccirati, All purpose numerical evaluation of one loop multileg Feynman diagrams, *Nucl. Phys.* B650 (2003) 162–228. arXiv:hep-ph/0209219, doi:10.1016/S0550-3213(02)01070-2. (3, 4, 5, 23, 26, 34, 37)
- [52] D. B. Melrose, Reduction of Feynman diagrams, *Nuovo Cim.* 40 (1965) 181–213. doi:10.1007/BF02832919. (4, 26, 28)
- [53] T. Regge, G. Barucchi, On the properties of Landau curves, *Il Nuovo Cimento* (1955-1965) 34 (1) (1964) 106–140. doi:10.1007/BF02725874.
URL <https://doi.org/10.1007/BF02725874> (4, 5)
- [54] J. Fleischer, T. Riemann, V. Yundin, One-Loop Tensor Feynman Integral Reduction with Signed Minors, *J. Phys. Conf. Ser.* 368 (2012) 012057. arXiv:1112.0500, doi:10.1088/1742-6596/368/1/012057. (4, 5)
- [55] S. Gorla, G. Passarino, Anomalous Threshold as the Pivot of Feynman Amplitudes, *Nucl. Phys. Proc. Suppl.* 183 (2008) 320–325. arXiv:0807.0698, doi:10.1016/j.nuclphysbps.2008.09.124. (4)
- [56] T. Sakkalis, R. Farouki, Singular points of algebraic curves, *Journal of Symbolic Computation* 9 (4) (1990) 405 – 421. doi:https://doi.org/10.1016/S0747-7171(08)80019-3.
URL <http://www.sciencedirect.com/science/article/pii/S0747717108800193> (4)
- [57] R. J. Eden, P. V. Landshoff, D. I. Olive, J. C. Polkinghorne, *The analytic S-matrix*, Cambridge Univ. Press, Cambridge, 1966. (4, 5)
- [58] R. Hwa, V. Teplitz, *Homology and Feynman Integrals*, Mathematical physics monograph series, W. A. Benjamin, 1966.
URL <https://books.google.it/books?id=uGZmb9M4xs4C> (4)
- [59] E. R. Speer, M. J. Westwater, *Generic Feynman amplitudes*. (4)
- [60] F. V. Tkachov, Landau equations and asymptotic operation, *Int. J. Mod. Phys. A* 14 (1999) 683–715. arXiv:hep-ph/9703423, doi:10.1142/S0217751X99000348. (5)
- [61] S. Abreu, R. Britto, C. Duhr, E. Gardi, Cuts from residues: the one-loop case, *JHEP* 06 (2017) 114. arXiv:1702.03163, doi:10.1007/JHEP06(2017)114. (5)
- [62] T. Dennen, M. Spradlin, A. Volovich, Landau Singularities and Symbology: One- and Two-loop MHV Amplitudes in SYM Theory, *JHEP* 03 (2016) 069. arXiv:1512.07909, doi:10.1007/JHEP03(2016)069. (5)
- [63] P. Chin, E. T. Tomboulis, Nonlocal vertices and analyticity: Landau equations and general Cutkosky rules arXiv:1803.08899. (5)
- [64] J. Maldacena, D. Simmons-Duffin, A. Zhiboedov, Looking for a bulk point, *JHEP* 01 (2017) 013. arXiv:1509.03612, doi:10.1007/JHEP01(2017)013. (5)
- [65] R. E. Cutkosky, Singularities and discontinuities of Feynman amplitudes, *J. Math. Phys.* 1 (1960) 429–433. doi:10.1063/1.1703676. (5, 26)
- [66] S. Mandelstam, Unitarity Condition Below Physical Thresholds in the Normal and Anomalous Cases, *Phys. Rev. Lett.* 4 (1960) 84–87.

- doi:10.1103/PhysRevLett.4.84. (5)
- [67] R. Pius, A. Sen, Unitarity of the Box Diagram [arXiv:1805.00984](#). (5)
- [68] A. Denner, S. Dittmaier, Scalar one-loop 4-point integrals, *Nucl. Phys. B* 844 (2011) 199–242. [arXiv:1005.2076](#), doi:10.1016/j.nuclphysb.2010.11.002. (5)
- [69] A. Denner, S. Dittmaier, Reduction schemes for one-loop tensor integrals, *Nucl. Phys. B* 734 (2006) 62–115. [arXiv:hep-ph/0509141](#), doi:10.1016/j.nuclphysb.2005.11.007. (5)
- [70] J. Bernstein, Modules over a ring of differential operators, *Functional Anal. App.* 5(2) (1971) 89–101. (6)
- [71] M. Sato, Theory of prehomogeneous vector spaces (algebraic part), *Nagoya Mat. J.* 120 (1990) 1–34. (6)
- [72] F. V. Tkachov, Algebraic algorithms for multiloop calculations. The First 15 years. What's next?, *Nucl. Instrum. Meth. A* 389 (1997) 309–313. [arXiv:hep-ph/9609429](#), doi:10.1016/S0168-9002(97)00110-1. (6)
- [73] G. 't Hooft, M. J. G. Veltman, Scalar One Loop Integrals, *Nucl. Phys. B* 153 (1979) 365–401. doi:10.1016/0550-3213(79)90605-9. (7)
- [74] J. A. John, N. R. Draper, An alternative family of transformations, *Journal of the Royal Statistical Society. Series C (Applied Statistics)*, vol. 29, no. 2 (1980). (7, 11)
- [75] D. D. Brayshaw, W. A. Simmons, S. F. Tuan, Some comments on the Brayshaw mechanism for generating peaks in the hadron system, *Phys. Rev. D* 18 (1978) 1719. doi:10.1103/PhysRevD.18.1719. (8)
- [76] S. F. Tuan, The Brayshaw Mechanism for Generating Peaks in the Hadron System, in: *High energy physics. Proceedings, 19th International Conference, ICHEP 1978, Tokyo, Japan, August 23-August 30, 1978, 1979*, pp. 137–139. URL <http://inspirehep.net/record/137636/files/c78-08-23-p137.pdf> (8)
- [77] N. Kauer, G. Passarino, Inadequacy of zero-width approximation for a light Higgs boson signal, *JHEP* 1208 (2012) 116. [arXiv:1206.4803](#), doi:10.1007/JHEP08(2012)116. (8)
- [78] F. Caola, K. Melnikov, Constraining the Higgs boson width with ZZ production at the LHC, *Phys. Rev. D* 88 (2013) 054024. [arXiv:1307.4935](#), doi:10.1103/PhysRevD.88.054024. (8)
- [79] S. Actis, G. Passarino, Two-Loop Renormalization in the Standard Model Part III: Renormalization Equations and their Solutions, *Nucl. Phys. B* 777 (2007) 100–156. [arXiv:hep-ph/0612124](#), doi:10.1016/j.nuclphysb.2007.04.027. (8)
- [80] R. Peierls, *Model-Making in Physics*, 2012, pp. 718–732. doi:10.1142/9789812795779_0066. URL https://www.worldscientific.com/doi/abs/10.1142/9789812795779_0066 (8)
- [81] H. P. Stapp, Discontinuity Formulas for Multiparticle Amplitudes, in: *Ecole d'Ete de Physique Theorique - Methods in Field Theory Les Houches, France, July 28-September 6, 1975, 1976*, p. 191. (8)
- [82] G. Passarino, C. Sturm, S. Uccirati, Higgs Pseudo-Observables, Second Riemann Sheet and All That, *Nucl. Phys. B* 834 (2010) 77–115. [arXiv:1001.3360](#), doi:10.1016/j.nuclphysb.2010.03.013. (8, 28)
- [83] B. Carlson, Numerical computation of real or complex elliptic integrals, *Numerical Algorithms* 10, no. 1 (1995) 13–26. (9)
- [84] C. Chandler, H. P. Stapp, Macroscopic causality conditions and properties of scattering amplitudes, *J. Math. Phys.* 10 (1969) 826–859. doi:10.1063/1.1664913. (9)
- [85] D. Iagolnitzer, H. P. Stapp, Macroscopic causality and physical region analyticity in S-matrix theory, *Commun. Math. Phys.* 14 (1969) 15–55. doi:10.1007/BF01645454. (9, 32)
- [86] J. Coster, H. P. Stapp, Physical-region discontinuity equations for many-particle scattering amplitudes. 1., *J. Math. Phys.* 10 (1969) 371–396. doi:10.1063/1.1664852. (9)
- [87] J. Coster, H. P. Stapp, Physical-region discontinuity equations for many-particle scattering amplitudes. 2., *J. Math. Phys.* 11 (1970) 1441–1463. doi:10.1063/1.1665279. (9)
- [88] T. Regge, Old Problems and New Hopes in S Matrix Theory, *Publ. Res. Inst. Math. Sci. Kyoto* 12 (1977) 367–375. doi:10.2977/prims/1195196616. (9)
- [89] A. White, The Past and future of S matrix theory (2000) 1483–1504 [arXiv:hep-ph/0002303](#). (9)
- [90] S. Gorla, G. Passarino, D. Rosco, The Higgs Boson Lineshape, *Nucl. Phys. B* 864 (2012) 530–579. [arXiv:1112.5517](#), doi:10.1016/j.nuclphysb.2012.07.006. (12)
- [91] R. Kumar, Covariant phase-space calculations of n-body decay and production processes, *Phys. Rev.* 185 (1969) 1865–1875. doi:10.1103/PhysRev.185.1865. (14, 17, 26, 27, 34, 36)
- [92] G. Passarino, Unnaturalness in the Higgs fermion sector, *Phys. Lett. B* 195 (1987) 191–194. doi:10.1016/0370-2693(87)91192-0. (15)
- [93] G. Passarino, Higgs Boson Production and Decay: Dalitz Sector, *Phys. Lett. B* 727 (2013) 424–431. [arXiv:1308.0422](#), doi:10.1016/j.physletb.2013.10.052. (15)
- [94] G. Bonnevey, I. J. R. Aitchison, J. S. Dowker, Analytic properties of the three point function, *Il Nuovo Cimento* (1955-1965) 21 (6) (1961) 1001–1011. doi:10.1007/BF02748059. URL <https://doi.org/10.1007/BF02748059> (28)
- [95] L. M. Brown, Analytic properties of n-point loops in perturbation theory, *Nuovo Cim.* 22 (1) (1961) 178–182. doi:10.1007/BF02829004. (28)
- [96] V. E. Asribekov, Choice of Invariant Variables for the "Many-Point" Functions, *J. Exp. Theor. Phys.* 15 (2) (1962) 394. (28)
- [97] A. Ferroglia, M. Passera, G. Passarino, S. Uccirati, Two loop vertices in quantum field theory: Infrared convergent scalar configurations, *Nucl. Phys. B* 680 (2004) 199–270. [arXiv:hep-ph/0311186](#), doi:10.1016/j.nuclphysb.2003.12.016. (28)
- [98] S. Heinemeyer, C. Schappacher, Higgs Decays into Charginos and Neutralinos in the Complex MSSM: A Full One-Loop Analysis, *Eur. Phys. J. C* 75 (5) (2015) 230. [arXiv:1503.02996](#), doi:10.1140/epjc/s10052-015-3442-5. (31)
- [99] A. David, G. Passarino, How well can we guess theoretical uncertainties?, *Phys. Lett. B* 726 (2013) 266–272. [arXiv:1307.1843](#), doi:10.1016/j.physletb.2013.08.025. (32)
- [100] M. J. G. Veltman, Unitarity and causality in a renormalizable field theory with unstable particles, *Physica* 29 (1963) 186–207. (32)
- [101] H. Weldon, The Description of Unstable Particles in Quantum Field Theory, *Phys. Rev. D* 14 (1976) 2030. doi:10.1103/PhysRevD.14.

2030. (32)